

A founder mutation in EHD1 presents with tubular proteinuria and deafness

Journal:	<i>Journal of the American Society of Nephrology</i>
Manuscript ID	JASN-2021-10-1312.R1
Manuscript Type:	Original Article - Basic Research
Date Submitted by the Author:	17-Dec-2021
Complete List of Authors:	<p>Issler, Naomi; University College London, Department of Renal Medicine Afonso, Sara; University of Regensburg, Medical Cell Biology; Friedrich-Alexander University Erlangen-Nuremberg, Physiology Weissman, Irith; Galilee Medical Center Jordan, Katrin; University of Regensburg, Medical Cell Biology Cebrian-Serrano, Alberto; University of Oxford, Wellcome Trust Centre for Human Genetics Meindl, Katrin; University of Regensburg, Medical Cell Biology Dahlke, Eileen; Kiel University, Institute of Anatomy Tziridis, Konstantin; Friedrich-Alexander University Erlangen-Nuremberg, ENT Clinic, University Hospital Erlangen Yan, Guanhua; The University of Manchester, Division of Molecular & Cellular Function Robles-López, José M.; The University of Manchester, Division of Molecular & Cellular Function Tabernero, Lydia; The University of Manchester, Division of Infection, Immunity and Respiratory Medicine Patel, Vaksha; University College London, Department of Renal Medicine Kesselheim, Anne; University College London, Department of Renal Medicine Klootwijk, Riko; University College London, Department of Renal Medicine Stanescu, Horia; University College London, Department of Renal Medicine Dumitriu, Simona; University College London, Department of Renal Medicine Iancu, Daniela; University College London, Department of Renal Medicine Tekman, Mehmet; University College London, Department of Renal Medicine Mozere, Monika; University College London, Department of Renal Medicine Jaureguiberry, Graciana; University College London, Department of Renal Medicine Ottandy, Priya; University College London, Department of Renal Medicine Russell, Claire; The Royal Veterinary College, Department of Comparative Biomedical Sciences Forst, Anna-Lena; University of Regensburg, Medical Cell Biology Sterner, Christina; University of Regensburg, Medical Cell Biology Heinl, Elena-Sofia; University of Regensburg, Medical Cell Biology</p>

1
2
3
4
5
6
7
8
9
10
11
12
13
14
15
16
17
18
19
20
21
22
23
24
25
26
27
28
29
30
31
32
33
34
35
36
37
38
39
40
41
42
43
44
45
46
47
48
49
50
51
52
53
54
55
56
57
58
59
60

	<p>Othmen, Helga; University of Regensburg, Institute for Molecular and Cellular Anatomy; University of Regensburg, Medical Cell Biology Tegtmeier, Ines; University of Regensburg, Medical Cell Biology Reichold, Markus; University of Regensburg, Medical Cell Biology Schiesl, Ina; University of Regensburg, Institute of Physiology; Aarhus University, Department of Biomedicine Limm, Katharina; University of Regensburg Faculty of Medicine, Functional Genomics Oefner, Peter; University of Regensburg Faculty of Medicine, Functional Genomics Witzgall, Ralph; University of Regensburg, Institute for Molecular and Cellular Anatomy Fu, Lifei; University of Regensburg, Biophysics II Theilig, Franziska; Christian-Albrechts-Universität zu Kiel Medizinische Fakultät, Institute of Anatomy Schilling, Achim; Friedrich-Alexander University Erlangen-Nuremberg, ENT Clinic, University Hospital Erlangen Biton, Efrat Shuster; Galilee Medical Center Kalfon, Limor; Galilee Medical Center Fedida, Ayalla; Galilee Medical Center Arnon-Sheleg, Elite; Galilee Medical Center Ben Izhak, Ofer; Rambam Health Care Campus, Pathology Institute Magen, Daniella; Rambam Health Care Campus, Pediatric Nephrology Institute Anikster, Yair; Sheba Medical Center Schulze, Holger; Friedrich-Alexander University Erlangen-Nuremberg, ENT Clinic, University Hospital Erlangen Ziegler, Christine; University of Regensburg, Biophysics II Lowe, Martin; The University of Manchester, Division of Molecular & Cellular Function Davies, Ben; University of Oxford, Wellcome Trust Centre for Human Genetics Bockenhauer, Detlef; University College London, Department of Renal Medicine Kleta, Robert; University College London, Department of Renal Medicine Falik Zaccai, Tzipora C.; Galilee Medical Center Warth, Richard; University of Regensburg, Medical Cell Biology</p>
Keywords:	Epithelial transport physiology, Infertility, Megalin, Eps15 Homology Domain, proximal tubule, genetic renal disease, Mutation

SCHOLARONE™
Manuscripts

Authors: Issler, Naomi; Afonso, Sara; Weissman, Irith; Jordan, Katrin; Cebrian-Serrano, Alberto; Meindl, Katrin; Dahlke, Eileen; Tziridis, Konstantin; Yan, Guanhua; Robles-López, José M.; Taberner, Lydia; Patel, Vaksha; Kesselheim, Anne; Klootwijk, Riko; Stanescu, Horia; Dumitriu, Simona; Iancu, Daniela; Tekman, Mehmet; Mozere, Monika; Jaureguiberry, Graciana; Uttandy, Priya; Russell, Claire; Forst, Anna-Lena; Sterner, Christina; Heintz, Elena-Sofia; Othmen, Helga; Tegtmeier, Ines; Reichold, Markus; Schiessl, Ina; Limm, Katharina; Oefner, Peter; Witzgall, Ralph; Fu, Lifei; Theilig, Franziska; Schilling, Achim; Biton, Efrat Shuster; Kalfon, Limor; Fedida, Ayalla; Arnon-Sheleg, Elite; Ben Izhak, Ofer; Magen, Daniella; Anikster, Yair; Schulze, Holger; Ziegler, Christine; Lowe, Martin; Davies, Ben; Bockenhauer, Detlef; Kleta, Robert; Falik Zaccai, Tzipora C.; Warth, Richard

Title: A founder mutation in EHD1 presents with tubular proteinuria and deafness

Running title: Proteinuria, deafness and EHD1

Manuscript Type: Original Article - Basic Research

Manuscript Category: Cell and transport physiology

Funders: Kids Kidney Research, (Grant / Award Number:)
 Grocers' Charity, (Grant / Award Number:)
 St Peter's Trust for Kidney, Bladder & Prostate Research, (Grant / Award Number:)
 Erasmus Program, (Grant / Award Number:)
 David and Elaine Potter Charitable Foundation, (Grant / Award Number:)
 Mitchell Charitable Trust, (Grant / Award Number:)
 NIHR Biomedical Research Centre at GOSH/ICH, (Grant / Award Number:)
 Wellcome Trust, (Grant / Award Number: '203141/Z/16/Z')
 Kidney Research UK, (Grant / Award Number:)
 DFG, German Research Foundation, (Grant / Award Number: '387509280','SFB 1350')
 Lowe Syndrome Trust, (Grant / Award Number: 'MU/ML/2016')

Financial Disclosure: CUST_FINANCIAL_DISCLOSURE :No data available. The authors have nothing to disclose.

Study Group/Organization Name: CUST_STUDY_GROUP/ORGANIZATION_NAME :No data available.

Study Group Members' Names: CUST_STUDY_GROUP_MEMBERS :No data available.

Total number of words: 3207

Abstract: Background:

The endocytic reabsorption of proteins in the proximal tubule requires a complex machinery and defects can lead to tubular proteinuria. The precise mechanisms of endocytosis and processing of receptors and cargo are incompletely understood. EHD1 belongs to a family of proteins presumably involved in the scission of intracellular vesicles and in ciliogenesis. However, the relevance of EHD1 in human tissues, in particular the kidney, was unknown.

Methods:

1
2
3 Genetic techniques were used in patients with tubular proteinuria and deafness to identify the disease-
4 causing gene. Diagnostic and functional studies were performed in patients and disease models to
5 investigate the pathophysiology.

6 Results:

7 We identified six individuals (5-33 years) with proteinuria and a high-frequency hearing deficit
8 associated with the homozygous missense variant c.1192C>T (p.R398W) in EHD1. Proteinuria (0.7-2.1
9 g/d) consisted predominantly of low-molecular-weight proteins, reflecting impaired renal proximal
10 tubular endocytosis of filtered proteins. Ehd1 knockout and Ehd1R398W/R398W knockin mice also
11 showed a high-frequency hearing deficit and impaired receptor-mediated endocytosis in proximal
12 tubules, and a zebrafish model showed impaired ability to reabsorb low-molecular-weight dextran.
13 Interestingly, ciliogenesis appeared unaffected in patients and mouse models. In silico structural analysis
14 predicted a destabilizing effect of the R398W variant and possible inference with nucleotide-binding
15 leading to impaired EHD1 oligomerization and membrane remodeling ability.

16 Conclusion:

17 A previously unrecognized autosomal recessive disorder characterized by sensorineural deafness and
18 tubular proteinuria is caused by a homozygous missense variant in EHD1. Recessive EHD1 variants
19 should be considered in individuals with hearing impairment, especially if tubular proteinuria is noted.
20
21
22
23
24
25
26
27
28
29
30
31
32
33
34
35
36
37
38
39
40
41
42
43
44
45
46
47
48
49
50
51
52
53
54
55
56
57
58
59
60

Significance Statement

Renal tubular protein reabsorption has been the focus of interest in the kidney community, and despite numerous associated inherited diseases, the detailed molecular basis remains poorly understood. Based on six patients with tubular proteinuria and sensorineural hearing deficit, EHD1 was identified as a critical component of the renal protein reabsorption machinery and inner ear function. As a key player in vesicular dynamics, EHD1 has previously been associated with early ciliogenesis. However, no obvious defect of ciliogenesis was found in the kidney of either the patients studied here or in knockin and knockout mice. In summary, these data may contribute to a better understanding of the functional relevance of EHD1 in human tissues, particularly in the kidney and inner ear.

A founder mutation in EHD1 presents with tubular proteinuria and deafness

Running title: Proteinuria, deafness and EHD1

Naomi Issler ^{1#}, Sara Afonso ^{2#}, Irith Weissman ^{3#}, Katrin Jordan ², Alberto Cebrian-Serrano ⁴, Katrin Meindl ², Eileen Dahlke ⁵, Konstantin Tziridis ⁶, Guanhua Yan ⁷, José M. Robles-López ⁷, Lydia Tabernero ⁷, Vaksha Patel ¹, Anne Kesselheim ¹, Enriko D. Klootwijk ¹, Horia C. Stanescu ¹, Simona Dumitriu ¹, Daniela Iancu ¹, Mehmet Tekman ¹, Monika Mozere ¹, Graciana Jaureguiberry ¹, Priya Outtandy ¹, Claire Russell ⁷, Anna-Lena Forst ², Christina Sterner ², Elena-Sofia Heintz ², Helga Othmen ², Ines Tegtmeier ², Markus Reichold ², Ina Maria Schiessl ⁹, Katharina Limm ¹⁰, Peter Oefner ¹⁰, Ralph Witzgall ¹¹, Lifei Fu ¹², Franziska Theilig ⁵, Achim Schilling ⁶, Efrat Shuster Biton ³, Limor Kalfon ³, Ayalla Fedida ³, Elite Arnon-Sheleg ³, Ofer Ben Izhak ¹³, Daniella Magen ¹³, Yair Anikster ¹⁴, Holger Schulze ⁶, Christine Ziegler ¹², Martin Lowe ⁷, Benjamin Davies ⁴, Detlef Böckenhauer ¹, Robert Kleta ^{1*#}, Tzipora C. Falik Zaccai ^{3#}, Richard Warth ^{2*#}

contributed equally

- ¹ Department of Renal Medicine, UCL, London, UK
- ² Medical Cell Biology, University Regensburg, Germany
- ³ Galilee Medical Center, Nahariya, Israel
- ⁴ Wellcome Centre Human Genetics, University Oxford, UK
- ⁵ Institute of Anatomy, University Kiel, Germany
- ⁶ ENT Clinic, University Hospital Erlangen, Germany
- ⁷ Division of Molecular & Cellular Function, University Manchester, UK
- ⁸ Royal Veterinary College, London, UK
- ⁹ Institute of Physiology, University Regensburg, Germany
- ¹⁰ Institute of Functional Genomics, University Regensburg, Germany
- ¹¹ Molecular and Cellular Anatomy, University Regensburg, Germany
- ¹² Structural Biology, University Regensburg, Germany
- ¹³ Pediatric Nephrology Institute, Haifa, Israel
- ¹⁴ Sheba Medical Center, Tel-Aviv, Israel

*Corresponding authors:

Robert Kleta, MD/PhD
Potter Chair of Nephrology
Department of Renal Medicine
University College London
Rowland Hill Street, London NW3 2PF, UK
phone: ++44-20 7314 7554
email: r.kleta@ucl.ac.uk

Richard Warth, MD
Medical Cell Biology
University Regensburg
Universitaetsstr. 31, 93053 Regensburg,
Germany
phone: ++49 941 943 2894
email: richard.warth@ur.de

Key words:

Epithelial transport physiology, Infertility, Megalin, Eps15 Homology Domain, proximal tubule, genetic renal disease

Abstract

Background: The endocytic reabsorption of proteins in the proximal tubule requires a complex machinery and defects can lead to tubular proteinuria. The precise mechanisms of endocytosis and processing of receptors and cargo are incompletely understood. EHD1 belongs to a family of proteins presumably involved in the scission of intracellular vesicles and in ciliogenesis. However, the relevance of EHD1 in human tissues, in particular the kidney, was unknown.

Methods: Genetic techniques were used in patients with tubular proteinuria and deafness to identify the disease-causing gene. Diagnostic and functional studies were performed in patients and disease models to investigate the pathophysiology.

Results: We identified six individuals (5-33 years) with proteinuria and a high-frequency hearing deficit associated with the homozygous missense variant c.1192C>T (p.R398W) in *EHD1*. Proteinuria (0.7-2.1 g/d) consisted predominantly of low-molecular-weight proteins, reflecting impaired renal proximal tubular endocytosis of filtered proteins. *Ehd1* knockout and *Ehd1*^{R398W/R398W} knockin mice also showed a high-frequency hearing deficit and impaired receptor-mediated endocytosis in proximal tubules, and a zebrafish model showed impaired ability to reabsorb low-molecular-weight dextran. Interestingly, ciliogenesis appeared unaffected in patients and mouse models. *In silico* structural analysis predicted a destabilizing effect of the R398W variant and possible inference with nucleotide-binding leading to impaired EHD1 oligomerization and membrane remodeling ability.

Conclusion: A previously unrecognized autosomal recessive disorder characterized by sensorineural deafness and tubular proteinuria is caused by a homozygous missense variant in *EHD1*. Recessive *EHD1* variants should be considered in individuals with hearing impairment, especially if tubular proteinuria is noted.

Introduction

Endocytosis refers to the mechanism by which cells internalize macromolecules and particles into transport vesicles derived from the plasma membrane¹. It is a crucial and regulated pathway for entry into the cell involved in numerous processes, including neurotransmission, signal transduction, immune response and cellular homeostasis. In the kidney, endocytosis is critical for the reabsorption of filtered macromolecules, such as LMW proteins. Investigations of rare diseases associated with LMW proteinuria have identified important roles for several cellular proteins involved in this process. Most filtered macromolecules are retrieved from the proximal tubular lumen by the promiscuous receptors Megalin, Cubilin and Amnionless², Mutations in the encoding genes *LRP2*, *CUBN* and *AMN* cause Donnai-Barrow syndrome (MIM222448) and Imlerslund-Grasbeck syndrome (MIM261100 and 618882), respectively³⁻⁵. Following endocytosis and release of cargo in the endosome, the receptors are recycled to the plasma membrane, while the cargo is transported to its downstream destination, either the lysosome (degradation) or the basolateral membrane (transepithelial transport)². An important regulator of this sorting process is the phosphatidylinositol 5'-phosphatase OCRL, mutations in which cause Lowe syndrome (MIM309000), whereas the chloride/proton antiporter CLCN5 is involved in endosomal acidification and constitutes the molecular basis of Dent disease (MIM300009); both clinically showing LMW proteinuria⁶.

Here we report on our investigations related to patients who presented with LMW proteinuria and sensorineural deafness with neither pathogenic variants in known disease genes nor other defining phenotypes associated with these known disorders. Instead, genetic analysis revealed a homozygous missense mutation in the *EHD1* gene.

EHD1 is one of four mammalian dynamin-like C-terminal Eps15 Homology Domain (EHD) proteins and localized to several cytoplasmic vesicular structures, including endocytic vesicles and the Golgi apparatus⁷. The EHD proteins have been previously implicated in endosomal scission, so that receptor

1
2
3 and cargo can be separated in order to be processed to their respective proper destinations^{8,9}. Yet,
4
5 studies in knockout mice have yielded variable results, ranging from a subclinical phenotype to
6
7 abnormal sperm development to eye abnormalities to impaired ciliogenesis to embryonic lethality¹⁰⁻
8
9
10¹⁴. Interestingly, none of these studies found a role for EHD1 in the kidney or inner ear.
11
12
13
14
15
16
17
18
19
20
21
22
23
24
25
26
27
28
29
30
31
32
33
34
35
36
37
38
39
40
41
42
43
44
45
46
47
48
49
50
51
52
53
54
55
56
57
58
59
60

Methods

Full details of all methods can be found in the Supplement.

Ethics

The study was performed in accordance with the Declaration of Helsinki. It was approved by the IRB of the Galilee Medical Center in Naharia (study # 06022007), and by the supreme Helsinki committee of the Israeli Ministry of Health (study # 920070611). The first patient was recruited on May 1st 2008, the last patient was recruited on July 11th 2018. Informed consent was obtained directly from the adult participant and from the parents of participants aged 18 years and younger. *Druze* ethnicity was self-reported by participants and is reported because of its potential impact on the frequency of genetic variants. All clinical examinations and investigations were performed at the discretion of the treating clinician as part of the patients' diagnosis and treatment.

Genetic studies

Genotyping, linkage studies and whole exome sequencing were performed as described previously¹⁵. Variants were assessed using a custom-built in-house software pipeline¹⁶, as well as the Ingenuity platform (<https://variants.ingenuity.com/qci/>).

Animal models

Experiments were performed according to the guidelines for the care and use of laboratory animals published by the US National Institutes of Health and were approved by the local councils for animal care. *Ehd1* knockout mice were generated by the Sanger Institute, as described previously¹⁷ and acquired from the European Mouse Mutant Archive (MGI ID: 4432418). *Ehd1* knockin mice were generated at the Wellcome Trust Centre for Human Genetics, University of Oxford, United Kingdom. Animal experiments on mice to assess renal function were approved by the "Regierung Unterfranken",

1
2
3 Germany. Zebrafish were studied for renal tubular LMW dextran handling as described previously¹⁸.

4
5 For details please see the Supplement.
6
7
8
9

10 Renal elimination of labelled β_2 -microglobulin

11
12 A recombinant human β_2 -microglobulin expressed in *E. coli* (Merck, #475828) was conjugated with
13
14 the fluorescent tag Alexa Fluor™ 546 and injected into anesthetized mice. After 30 min, urine and
15
16 blood were collected and tissue fixation was performed. The fluorescence of β_2 -microglobulin-Alexa
17
18 Fluor 546 in urine, serum and kidney lysate samples was measured.
19
20
21
22

23 Intravital imaging of proximal tubular protein reabsorption

24
25 Mice were anesthetized and the left kidney was exposed. To label the vasculature, a 25 mg/ml solution
26
27 of FITC-500 kDa Dextran conjugate was used. After 1 min β_2 -microglobulin-Alexa Fluor 546 was
28
29 injected intravenously and the proximal tubular uptake was measured as increase in tubular
30
31 fluorescence intensity (up to 30 min after injection).
32
33
34
35
36

37 Auditory brainstem response measurements

38
39 Anesthetized mice aged 6-9 weeks were used for the measurement of the auditory brainstem
40
41 response. Stimuli presented were pure tones at 4, 8, 16 and 32 kHz.
42
43
44
45

46 Statistics

47
48 Data are shown as mean values \pm standard error of the mean (SEM); “n” stands for the number of
49
50 observations. Two-sided unpaired Student’s t-test and ANOVA were used to calculate significance
51
52 between different groups as appropriate. A p-value \leq 0.05 was accepted to indicate statistical
53
54 significance.
55
56
57
58
59
60

Results

Patients

We identified six individuals from four families with an unexplained unique phenotype of LMW proteinuria and sensorineural hearing loss. Proteinuria was discovered incidentally by dipstick (trace to 2+) during investigations for minor illnesses. Four individuals had kidney biopsies performed due to proteinuria, which all were reported as being normal (Figure 1). Renal ultrasound studies showed normal findings. Proteinuria was noted to contain highly elevated levels of LMW protein, including β_2 -microglobulin and retinol binding protein, consistent with a defect in proximal tubular protein re-uptake (Figure 1 and Supplemental Table 1).

One individual had a DMSA scan because of suspected urinary tract infection which surprisingly showed globally impaired uptake of the tracer by the kidneys (Figure 1). Subsequently, other affected individuals also underwent DMSA scans with similarly impaired uptake.

The hearing problem was identified during the clinical work-up for this disorder. Audiograms in affected individuals revealed high-frequency hearing loss, consistent with sensorineural hearing impairment (Figure 1).

All affected individuals underwent detailed clinical examinations including formal neurological and ophthalmological assessments and no other abnormalities were identified. No dysmorphologies were noted. Blood studies for renal glomerular function including Vitamin B12 showed no abnormalities.

One individual became pregnant and delivered a healthy child. No affected male has so far had progeny. All individuals belong to a *Druze* ethnic-religious group in Palestine (pedigrees Figure 2).

Genetic studies

Linkage analysis identified a single significant region of interest comprising approximately 1.5 million bases on chromosome 11, with a significant LOD score of 7.2 (Figure 2). This small 1.5 cM locus was defined by two flanking SNPs: rs7131675 and rs2845570. Exome sequencing revealed in the linked

1
2
3 interval a single homozygous variant that segregated with the phenotype, located in *EHD1*: c.1192C>T;
4 p.(R398W). The damage prediction algorithms indicated functional impairment: CADD score: 32 (likely
5 deleterious); SIFT: 0.01 (deleterious); Polyphen: 0.677 (possibly damaging). This variant is also
6 annotated as rs151119199 in dbSNP (<https://www.ncbi.nlm.nih.gov/snp/>) and has an allele frequency
7 of 0.00001427 in the gnomAD database (<https://gnomad.broadinstitute.org>, accessed June 2021).
8 Sequencing of genetically matched healthy *Druze* individuals identified this variant in one of 196
9 alleles indicating a strongly increased allele frequency in this population.
10
11
12
13
14
15
16
17
18
19
20

21 EHD1 and kidney

22
23 In human kidney, we identified EHD1 predominantly in the subapical compartment of proximal
24 tubular epithelial cells (Figure 3 and Supplemental Figure 1). This was confirmed in mouse kidney,
25 where Ehd1 partially co-localized with the endocytic tracer β_2 -microglobulin and the apical receptor
26 proteins Megalin and Cubilin (Figure 4 and Supplemental Figures 2 and 3). Interestingly, localization
27 and abundance of Megalin and Cubilin appeared unaffected by Ehd1 knockout and knockin (Figure 4
28 and Supplemental Figure 6). *Ehd1* knockout and antibody specificity were confirmed by the presence
29 or absence of Ehd1 staining in wildtype and *Ehd1*^{-/-} mice, respectively (Supplemental Figure 2).
30
31
32
33
34
35
36
37
38

39 For functional assessment we first assessed *ehd1* in zebrafish. There are two orthologues in zebrafish
40 *ehd1a* and *ehd1b*, both of which are expressed in kidney. When suppressing both paralogues with
41 morpholinos, morphant zebrafish larvae had a significantly impaired ability to reabsorb low-molecular
42 weight dextran compared to control larvae (Supplemental Figure 4).
43
44
45
46
47

48 For a more detailed assessment, we investigated *Ehd1* knockout mice (*Ehd1*^{-/-}). We first measured
49 LMW protein uptake using fluorescently labelled β_2 -microglobulin. This showed a substantial decrease
50 in re-uptake in *Ehd1*^{-/-} versus wildtype mice resulting in increased urinary excretion (Figure 3). For
51 better assessment of the R398W variant identified in our patients, we also generated R398W knockin
52 mice (*Ehd1*^{R398W/R398W}). Mutant Ehd1 protein appeared to have largely decreased expression in
53
54
55
56
57
58
59
60

1
2
3 proximal tubules and was predominantly localized in small intracellular aggregates (Figure 4,
4 Supplemental Figure 5). In distal nephron segments, mutant Ehd1 was also present in elongated
5
6 elongated structures that were negative for acetylated tubulin, a marker for cilia (Supplemental Figure 5). These
7
8 elongated apical structures were not found in wildtype kidneys. In order to gain more mechanistic
9
10 insights, a possible effect of Ehd1 inactivation on Arf6 and Rab11, two factors involved in trafficking
11
12 of membranes, was examined. Interestingly, localization and abundance of Arf6 and Rab11 appeared
13
14 normal in proximal tubules of knockout and knockin mice (Supplemental Figures 6 and 7). Consistent
15
16 with our patients and *Ehd1*^{-/-} mice, *Ehd1*^{R398W/R398W} mice had increased levels of fluorescent β_2 -
17
18 microglobulin in the urine (Figure 3). Moreover, whereas in wildtype mice reabsorbed fluorescent β_2 -
19
20 microglobulin was mainly confined to the early segments of proximal tubule, in the genetically
21
22 modified mice it was present throughout the proximal tubule, consistent with compensatory uptake
23
24 in later segments of the proximal tubule (Figure 3). Similarly, *in vivo* imaging of mouse kidneys using
25
26 multiphoton microscopy showed a significantly lower β_2 -microglobulin uptake rate in *Ehd1*^{-/-} mice
27
28 (Figure 3 and Supplemental Figure 8).
29
30
31
32
33
34
35
36

37 EHD1 and inner ear

38
39 Because of the sensorineural deafness of our patients, we investigated expression of Ehd1 in mouse
40
41 inner ear and identified strong expression in the stria vascularis (Figure 5). Knockout and knockin mice
42
43 had a loss and altered pattern of Ehd1 expression, respectively (Figure 5). Importantly, *Ehd1*^{R398W/R398W}
44
45 mice also displayed a significant high-frequency hearing impairment of 20-30 dB compared to age-
46
47 matched wildtype mice (Figure 5).
48
49
50
51

52 Cellular studies

53
54 We further investigated the cellular consequences of the R398W mutant EHD1 in a proximal tubular
55
56 cell line, LLC-PK1, genetically modified to either express wildtype or mutant EHD1 when induced with
57
58
59
60

1
2
3 tetracycline. Cells with wildtype EHD1 showed a spotted distribution pattern as described ¹⁹. In
4
5 contrast, mutated EHD1 expressing cells showed elongated tubular structures, presumably tubular
6
7 recycling endosomes, indicating an impairment of membrane fission events (Figure 6). EHD1 is a
8
9 component of a complex multi-protein membrane shaping machinery. Previous work has indicated
10
11 that EHD1 together with other proteins, e.g. Pacsin 2, MICAL-L1, and ARF6, functions in endosomal
12
13 recycling ¹⁹⁻²¹. Therefore, we investigated the effect of the EHD1^{R398W} mutation on the distribution of
14
15 MICAL-L1 and Pacsin 2. Interestingly, MICAL-L1 remained associated to EHD1 in cells overexpression
16
17 mutant EHD1 and similarly Pacsin 2. These data indicate that the elongated structures observed in
18
19 cells with mutant EHD1^{R398W} are in fact abnormal tubular recycling endosomes (Supplemental Figures
20
21
22
23 9 and 10).

24
25 We also investigated protein stability. After removal of tetracycline, levels of both wildtype and
26
27 mutant EHD1 were similar, but levels of mutant EHD1 reduced significantly faster, consistent with
28
29 impaired protein stability of mutant EHD1 (Figure 6). This finding is in agreement with the reduced
30
31 protein abundance observed in kidneys of *Ehd1* knockin mice (Supplemental Figures 2 and 5).
32
33
34
35

36 37 Role of Ehd1 in renal ciliogenesis

38
39 Due to the previously reported role of EHD1 in cilia formation, we assessed cilia morphology ^{14, 22, 23}.
40
41 Interestingly, primary cilia were present and appeared to have normal morphology within the
42
43 proximal tubule in affected individuals, knockout as well as knockin animals (Supplemental Figure 11)
44
45 ²⁴.
46
47
48
49

50 51 In silico structural modelling

52
53 Structural analysis identified the mutated EHD1 R398 as part of the α -helix 12, presumably involved
54
55 in oligomerization of EHD1 (Figure 7 and Supplemental Figures 12-14). Replacement of arginine with
56
57 tryptophan at this position is predicted to disrupt the stability of interactions between EHD1 dimers
58
59
60

1
2
3 leading to mechanically instable oligomerization and the inability to process membrane scission.
4

5 Another consequence of the R398W mutation is its possible inference with the nucleotide-binding
6
7 pocket of an adjacent EHD1 (Figure 7).
8
9
10
11
12
13
14
15
16
17
18
19
20
21
22
23
24
25
26
27
28
29
30
31
32
33
34
35
36
37
38
39
40
41
42
43
44
45
46
47
48
49
50
51
52
53
54
55
56
57
58
59
60

Discussion

Our work describes a previously unrecognized syndrome presenting with LMW proteinuria and sensorineural deafness. An isolated population provided us with the opportunity to investigate this *EHD1* related syndrome. The unambiguous identification of an identical homozygous genetic variant in four families from the same ethnic background strongly suggests the presence of a founder mutation, consistent with the apparent increased allele frequency of this *EHD1* missense variant in the *Druze* population.

Our clinical, genetic and molecular findings are fully compatible with partial or organ specific loss of *EHD1* function as disease mechanism, consistent with autosomal recessive inheritance. The gnomAD database shows that *EHD1* is highly constrained and that predicted loss of function variants are significantly less observed than expected (probability of loss of function intolerance = 0.98) suggesting that this ubiquitously expressed protein has a unique and critical biological function^{25, 26}. Arguably, complete loss of function may not be compatible with human life and the R398W variant potentially retains some functionality or heterozygous loss of function entails a reproductive disadvantage²⁶.

We provide compelling experimental evidence for the role of *EHD1* in biology by unequivocally linking it to a distinct human phenotype, i.e. to disease mechanisms related to renal proximal tubular endocytosis and sensorineural deafness. We demonstrate *EDH1* related kidney phenotypes in man, in zebrafish as well as in knockout and knockin mice. Impaired renal handling of LMW molecules is seen in our patients, in zebrafish as well as in mice with *Ehd1* dysfunction. Remarkably, the renal phenotype was milder in mice than in humans, and decreased absorptive capacity was evident only by administration of labeled β_2 -microglobulin. Furthermore, we provide evidence for *EDH1* related hearing deficits in man and mouse and we speculate that *EHD1* dysfunction may interfere with male

1
2
3 fertility based on corroborating data from *Ehd1* knockout and additional data from knockin mice
4
5 (Supplemental Table 2).
6
7
8
9

10 Our work identifies EHD1 as a critical component in the endocytic machinery of the renal proximal
11 tubule, aligned with previous work which established a role for EHD1 in endocytic scission and
12 recycling⁹. We noted elongated pathological tubular structures in LLC-PK1 cells expressing mutant
13 EHD1 providing yet another piece of circumstantial evidence for EHD1's role in membrane shaping
14 and fission (Figure 5). In the proximal tubule such scission divides and separates recycling tubules from
15 sorting endosomes, so that receptor proteins handling cargo proteins, such as Megalin can be recycled
16 back to the apical membrane, whereas the cargo proteins can be directed to their respective targets
17
18
19
20
21
22
23
24
25
26
27
28
29
30
31
32
33
34
35
36
37
38
39
40
41
42
43
44
45
46
47
48
49
50
51
52
53
54
55
56
57
58
59
60

27. We propose that these EHD1 related mechanisms explain the reduced capacity of proximal tubular endocytosis and subsequent "overflow" of LMW proteins into the urine. Results from our study are fully consistent with this particular role for EHD1 (Figure 7). Interestingly, localization and abundance of Megalin, Cubilin, Arf6 and Rab11 appeared unaffected in *Ehd1* knockout and knockin mice (Figure 4 and Supplemental Figures 6 and 7). These data suggest that *Ehd1* does not physically bind to these proteins, but that its inactivation or mutation slows down fission of recycling tubules and thus transport rates.

Our data and damage prediction algorithms, such as a CADD score of 32, indicated functional impairment of the p.R398W mutant. A closer look into publicly available structure biology databases revealed how the identified missense mutation p.R398W may impair EHD1 function. On the molecular level, *in silico* modelling suggested that the mutation hinders the formation of EHD1 oligomers necessary for association with endosomes and membrane scission (Figure 7)²⁸⁻³⁰. Thus, structural modeling supported a direct effect on scission and as consequence impaired processing of membranes, receptors and cargo. Moreover, the identified *EHD1* mutation can also interfere with the

1
2
3 nucleotide-binding site of an adjacent EHD1 (Figure 7). This particular mechanism was further
4 supported by the extensive tubulation observed in renal proximal tubular cells expressing mutant
5 EHD1 (Figure 6), which in fact is reminiscent of the cellular phenotype of ATPase-deficient mutant
6 T94A in *Ehd2*³¹. However, our data do not allow to specify the extent of loss of function for the disease
7 causing R398W variant, yet, the similarity in the phenotypes of *Ehd1*^{-/-} and *Ehd1*^{R398W/R398W} mice
8 strongly suggests that it indeed significantly impairs organ specific functions.
9
10
11
12
13
14
15
16
17
18

19 A search of the Shared Harvard Inner-Ear Laboratory Database (SHIELD) revealed that *Ehd1* is known
20 to be expressed in the mouse inner ear³². The association of EHD1 dysfunction with sensorineural
21 deafness and its expression in stria vascularis (Figure 5) highlights the important role of receptor-
22 mediated endocytosis in inner ear function, consistent with the deafness seen in Donnai-Barrow
23 syndrome, due to mutations in Megalin³. While the exact role of Megalin in inner ear function is still
24 unclear, it has been implicated in endocytosis in the endolymphatic sac with prominent expression in
25 vestibular dark cells as well as stria vascularis^{33, 34}.
26
27
28
29
30
31
32
33
34
35

36 Male *Ehd1* knockout mice have previously been shown to be infertile¹⁰. Our results corroborate this
37 and, importantly, male *Ehd1*^{R398W/R398W} mice are also infertile (Supplemental Table 2). However, if this
38 also applies to humans remains to be seen as the young ages of our male patients do not allow any
39 conclusions.
40
41
42
43
44
45
46
47

48 Of further interest is our finding of morphologically normal primary cilia in both patients and
49 genetically modified mice (Supplemental Figure 11) as this is in contrast to previous reports of defects
50 in ciliogenesis in zebrafish and *Ehd1* knockout mice^{14, 22, 23}. Ciliopathies typically present in the kidney
51 with cysts, which were not seen in this study. Our findings argue against an essential role of EHD1 in
52
53
54
55
56
57
58
59
60

1
2
3 ciliogenesis, at least in the kidney. Of note, defects in ciliogenesis in mice appeared to be dependent
4
5 on the genetic background of mice ^{13,14}.
6
7
8
9

10 In summary, a previously unrecognized syndrome, characterized by LMW proteinuria and
11
12 sensorineural deafness accompanied by markedly reduced DMSA uptake in renal imaging, is caused
13
14 by mutated *EHD1*. Our findings enable an accurate diagnosis, genetic testing and counselling for
15
16 affected individuals and families. Our findings are consistent with a role for EHD1 as an intracellular
17
18 membrane-shaping protein involved in vesicular trafficking and recycling. Our work also establishes
19
20 *EHD1* as a new deafness disease gene. Because of the subtlety of the kidney phenotype, which may
21
22 go unrecognized in clinical practice, *EHD1* variants should be considered in patients with apparent
23
24 isolated deafness. Moreover, our study suggests a possible role for *EHD1* in male infertility, thereby
25
26 corroborating a previous study ¹⁰.
27
28
29

30 The identification of mutated EHD1 being causative for a rare disease entity in an isolated population
31
32 with its well-defined phenotypes provides solid evidence for EHD1's real role in life. These insights
33
34 position EHD1 a) as reasonable biological target for the prevention of treatment (e.g. cancer drugs)
35
36 related renal toxicity linked to proximal tubular transport processes ³⁵, b) as protein of interest for an
37
38 improved understanding of the biology of inner ear function and hearing problems, and potentially
39
40 also c) for a role in male fertility.
41
42
43
44
45
46
47

48 **Author Contributions**

49 All authors together generated and gathered the patient, animal, genetic and molecular data and
50
51 analyzed the data. Drs. Robert Kleta, Tzipora C. Falik Zaccai, and Richard Warth vouch for the data and
52
53 the analysis. All authors helped writing the paper, and all together decided to publish this paper.
54
55
56
57
58
59
60

Acknowledgements

We are grateful to all of our patients and their families for their kind and significant engagement.

Disclosures

D. Magen reports Consultancy: Alnylam Pharmaceuticals; Research Funding: Alnylam Pharmaceuticals; and Honoraria: Alnylam Pharmaceuticals. B. Davies reports Advisory or Leadership Role: International Society of Transgenic Technologies. R. Warth reports Advisory or Leadership Role: Editorial Board of JASN and Pflügers Archive; and Other Interests or Relationships: Member of the German Society of Nephrology and German Physiological Society. P. Oefner reports Ownership Interest: PDL BioPharma Inc.; and Advisory or Leadership Role: Editorial Board of BioTechniques, Communicating Editor of Human Mutation, Editorial Board of BioMed Research International, Oncology Section, and Editorial Board of Metabolites. E. Klootwijk reports Patents or Royalties: New Zealand Pharmaceuticals. All remaining authors have nothing to disclose.

Funding

DB and RK were supported by the Mitchell Charitable Trust, Kids Kidney Research, Kidney Research UK, the Lowe Syndrome Trust, and the Grocers' Charity. RK was supported by the David and Elaine Potter Charitable Foundation. RK, DB, EDK and HCS were supported by St Peter's Trust for Kidney, Bladder & Prostate Research. DB is supported by the NIHR Biomedical Research Centre at GOSH/ICH. RW was supported by the Deutsche Forschungsgemeinschaft (DFG, German Research Foundation), project number 387509280, SFB 1350. ML and JR were supported by the Lowe Syndrome Trust (MU/ML/2016) and the Erasmus program, respectively. BD and AC-S were supported by the Wellcome Trust [203141/Z/16/Z].

1
2
3
4
5
6
7
8
9
10
11
12
13
14
15
16
17
18
19
20
21
22
23
24
25
26
27
28
29
30
31
32
33
34
35
36
37
38
39
40
41
42
43
44
45
46
47
48
49
50
51
52
53
54
55
56
57
58
59
60

Supplemental Material Table of Contents

(All Supplemental Material is organized in a single pdf-file)

Supplemental Methods

- Ehd1 knockout mice
- Ehd1R398W/R398W knockin mice
- Immunostaining
- Stimulated-Emission–Depletion (STED) super-resolution microscopy
- Fluorescent labeling of β 2-microglobulin
- Reabsorption of β 2-microglobulin
- RNAScope of kidneys
- Auditory brainstem response measurement
- Intravital microscopy of renal proximal tubular endocytosis
- Zebrafish strains and husbandry
- Zebrafish RNA isolation, RT-PCR and Q-PCR
- Morpholino injections into zebrafish
- Injection and analysis of endocytic tracer
- Western blotting of zebrafish larvae
- Ethics statement on Zebrafish experiments
- Proteomics
- Homology modelling of EHD1 and EHD1R398W
- Statistics

Supplemental Tables

- Supplemental Table 1: Clinical phenotype details
- Supplemental Table 2: Breeding statistics

Supplemental Figures

- Supplemental Figure 1: EHD1 in human kidney
- Supplemental Figure 2: Ehd1 in mouse kidney
- Supplemental Figure 3: Localization Ehd1, Megalin and reabsorbed β 2-microglobulin
- Supplemental Figure 4. Zebrafish
- Supplemental Figure 5: Localization of Ehd1R398W in mouse kidney
- Supplemental Figure 6: Localization of Ehd1 and Arf6 in mouse kidneys
- Supplemental Figure 7: Effect of Ehd1 knockout and knockin on the localization of Rab11
- Supplemental Figure 8: Intravital multiphoton microscopy
- Supplemental Figure 9: EHD1 and MICAL-L1 in EDH1-overexpressing LLC-PK1 cells
- Supplemental Figure 10: MICAL-L1 and Pacsin 2 in cells overexpressing EDH1R398W
- Supplemental Figure 11: Primary cilia in murine and human kidneys
- Supplemental Figure 12: Alignment of EHD1, EHD2 and EHD4
- Supplemental Figure 13: Structural modeling: Putative structure of EHD1 dimers
- Supplemental Figure 14: Structural modeling: Effects of the R398W mutation on EHD1 oligomerization

Supplemental References

References

1. Conner SD, Schmid SL: Regulated portals of entry into the cell. *Nature* 422: 37-44, 2003 doi: 10.1038/nature01451
2. Christensen EI, Birn H: Megalin and cubilin: multifunctional endocytic receptors. *Nat Rev Mol Cell Biol* 3: 256-266, 2002
3. Kantarci S, Al-Gazali L, Hill RS, Donnai D, Black GC, Bieth E, et al.: Mutations in LRP2, which encodes the multiligand receptor megalin, cause Donnai-Barrow and facio-oculo-acoustico-renal syndromes. *Nat Genet* 39: 957-959, 2007 doi: 10.1038/ng2063
4. Aminoff M, Carter JE, Chadwick RB, Johnson C, Grasbeck R, Abdelaal MA, et al.: Mutations in CUBN, encoding the intrinsic factor-vitamin B12 receptor, cubilin, cause hereditary megaloblastic anaemia 1. *Nat Genet* 21: 309-313, 1999 doi: 10.1038/6831
5. Tanner SM, Aminoff M, Wright FA, Liyanarachchi S, Kuronen M, Saarinen A, et al.: Amnionless, essential for mouse gastrulation, is mutated in recessive hereditary megaloblastic anemia. *Nat Genet* 33: 426-429, 2003 doi: 10.1038/ng1098
6. Eshbach ML, Weisz OA: Receptor-mediated endocytosis in the proximal tubule. *Annu Rev Physiol* 79: 425-448, 2017 doi: 10.1146/annurev-physiol-022516-034234
7. Mintz L, Galperin E, Pasmanik-Chor M, Tulzinsky S, Bromberg Y, Kozak CA, et al.: EHD1 - an EH-domain-containing protein with a specific expression pattern. *Genomics* 59: 66-76, 1999 doi: 10.1006/geno.1999.5800
8. Naslavsky N, Caplan S: EHD proteins: key conductors of endocytic transport. *Trends Cell Biol* 21: 122-131, 2011 doi: 10.1016/j.tcb.2010.10.003
9. Deo R, Kushwah MS, Kamerkar SC, Kadam NY, Dar S, Babu K, et al.: ATP-dependent membrane remodeling links EHD1 functions to endocytic recycling. *Nat Commun* 9: 5187, 2018 doi: 10.1038/s41467-018-07586-z
10. Rainey MA, George M, Ying G, Akakura R, Burgess DJ, Siefker E, et al.: The endocytic recycling regulator EHD1 is essential for spermatogenesis and male fertility in mice. *BMC Dev Biol* 10: 37, 2010 doi: 10.1186/1471-213X-10-37
11. Posey AD, Jr., Swanson KE, Alvarez MG, Krishnan S, Earley JU, Band H, et al.: EHD1 mediates vesicle trafficking required for normal muscle growth and transverse tubule development. *Dev Biol* 387: 179-190, 2014 doi: 10.1016/j.ydbio.2014.01.004
12. Arya P, Rainey MA, Bhattacharyya S, Mohapatra BC, George M, Kuracha MR, et al.: The endocytic recycling regulatory protein EHD1 is required for ocular lens development. *Dev Biol* 408: 41-55, 2015 doi: 10.1016/j.ydbio.2015.10.005
13. Rapaport D, Auerbach W, Naslavsky N, Pasmanik-Chor M, Galperin E, Fein A, et al.: Recycling to the plasma membrane is delayed in EHD1 knockout mice. *Traffic* 7: 52-60, 2006 doi: 10.1111/j.1600-0854.2005.00359.x
14. Bhattacharyya S, Rainey MA, Arya P, Mohapatra BC, Mushtaq I, Dutta S, et al.: Endocytic recycling protein EHD1 regulates primary cilia morphogenesis and SHH signaling during neural tube development. *Sci Rep* 6: 20727, 2016 doi: 10.1038/srep20727
15. Klootwijk ED, Reichold M, Helip-Wooley A, Tolaymat A, Broeker C, Robinette SL, et al.: Mistargeting of peroxisomal EHHADH and inherited renal Fanconi's syndrome. *N Engl J Med* 370: 129-138, 2014 doi: 10.1056/NEJMoa1307581
16. Mozere M, Tekman M, Kari J, Bockenbauer D, Kleta R, Stanescu H: OVAS: an open-source variant analysis suite with inheritance modelling. *BMC Bioinformatics* 19: 46, 2018 doi: 10.1186/s12859-018-2030-8
17. Skarnes WC, Rosen B, West AP, Koutsourakis M, Bushell W, Iyer V, et al.: A conditional knockout resource for the genome-wide study of mouse gene function. *Nature* 474: 337-342, 2011 doi: 10.1038/nature10163

18. Oltrabella F, Pietka G, Ramirez IB, Mironov A, Starborg T, Drummond IA, et al.: The Lowe syndrome protein OCRL1 is required for endocytosis in the zebrafish pronephric tubule. *PLoS Genet* 11: e1005058, 2015 doi: 10.1371/journal.pgen.1005058
19. Sharma M, Giridharan SS, Rahajeng J, Naslavsky N, Caplan S: MICAL-L1 links EHD1 to tubular recycling endosomes and regulates receptor recycling. *Mol Biol Cell* 20: 5181-5194, 2009 doi: 10.1091/mbc.E09-06-0535
20. Rahajeng J, Giridharan SS, Cai B, Naslavsky N, Caplan S: MICAL-L1 is a tubular endosomal membrane hub that connects Rab35 and Arf6 with Rab8a. *Traffic* 13: 82-93, 2012 doi: 10.1111/j.1600-0854.2011.01294.x
21. Giridharan SS, Cai B, Vitale N, Naslavsky N, Caplan S: Cooperation of MICAL-L1, syndapin2, and phosphatidic acid in tubular recycling endosome biogenesis. *Mol Biol Cell* 24: 1776-1715, 2013
22. Lu Q, Insinna C, Ott C, Stauffer J, Pintado PA, Rahajeng J, et al.: Early steps in primary cilium assembly require EHD1/EHD3-dependent ciliary vesicle formation. *Nat Cell Biol* 17: 228-240, 2015 doi: 10.1038/ncb3109
23. Xie S, Farmer T, Naslavsky N, Caplan S: MICAL-L1 coordinates ciliogenesis by recruiting EHD1 to the primary cilium. *J Cell Sci* 132, 2019 doi: 10.1242/jcs.233973
24. Sun S, Fisher RL, Bowser SS, Pentecost BT, Sui H: Three-dimensional architecture of epithelial primary cilia. *Proc Natl Acad Sci U S A* 116: 9370-9379, 2019 doi: 10.1073/pnas.1821064116
25. Karczewski KJ, Francioli LC, Tiao G, Cummings BB, Alfoldi J, Wang Q, et al.: The mutational constraint spectrum quantified from variation in 141,456 humans. *Nature* 581: 434-443, 2020 doi: 10.1038/s41586-020-2308-7
26. Lek M, Karczewski KJ, Minikel EV, Samocha KE, Banks E, Fennell T, et al.: Analysis of protein-coding genetic variation in 60,706 humans. *Nature* 536: 285-291, 2016 doi: 10.1038/nature19057
27. Verroust PJ, Birn H, Nielsen R, Kozyraki R, Christensen EI: The tandem endocytic receptors megalin and cubilin are important proteins in renal pathology. *Kidney Int* 62: 745-756, 2002
28. Lee DW, Zhao X, Scarselletta S, Schweinsberg PJ, Eisenberg E, Grant BD, et al.: ATP binding regulates oligomerization and endosome association of RME-1 family proteins. *J Biol Chem* 280: 17213-17220, 2005 doi: 10.1074/jbc.M412751200
29. Naslavsky N, Caplan S: C-terminal EH-domain-containing proteins: consensus for a role in endocytic trafficking, EH? *J Cell Sci* 118: 4093-4101, 2005 doi: 10.1242/jcs.02595
30. Moren B, Shah C, Howes MT, Schieber NL, McMahon HT, Parton RG, et al.: EHD2 regulates caveolar dynamics via ATP-driven targeting and oligomerization. *Mol Biol Cell* 23: 1316-1329, 2012 doi: 10.1091/mbc.E11-09-0787
31. Daumke O, Lundmark R, Vallis Y, Martens S, Butler PJ, McMahon HT: Architectural and mechanistic insights into an EHD ATPase involved in membrane remodelling. *Nature* 449: 923-927, 2007 doi: 10.1038/nature06173
32. Shen J, Scheffer DI, Kwan KY, Corey DP: SHIELD: an integrative gene expression database for inner ear research. *Database (Oxford)* 2015: bav071, 2015 doi: 10.1093/database/bav071
33. Arai M, Mizuta K, Saito A, Hashimoto Y, Iwasaki S, Watanabe T, et al.: Localization of megalin in rat vestibular dark cells and endolymphatic sac epithelial cells. *Acta Otolaryngol* 128: 627-633, 2008 doi: 10.1080/00016480701668531
34. Hosokawa S, Hosokawa K, Ishiyama G, Ishiyama A, Lopez IA: Immunohistochemical localization of megalin and cubilin in the human inner ear. *Brain Res* 1701: 153-160, 2018 doi: 10.1016/j.brainres.2018.09.016
35. Rolleman EJ, Melis M, Valkema R, Boerman OC, Krenning EP, de Jong M: Kidney protection during peptide receptor radionuclide therapy with somatostatin analogues. *Eur J Nucl Med Mol Imaging* 37: 1018-1031, 2010 doi: 10.1007/s00259-009-1282-y

Figures legends

Figure 1: Human phenotype

Shown are key phenotypical features noted in affected individuals. (A) Bar graphs illustrating proteinuria with horizontal dashed black lines indicating the upper limits of normal. 24-h urine protein excretion (left bar) ranges from 0.67 to 2.1 g/d. Proteinuria was predominantly low molecular weight proteinuria as indicated by the highly elevated levels of β_2 -microglobulin (middle bar) and retinol binding protein (RBP, normalized to urinary creatinine, right bar). (B) Affected individuals had impaired renal uptake of DMSA. Shown are representative single photon emission tomography (SPECT) images from a healthy control (left panel) and individual 1.1 (right panel) 4 hours after injection of DMSA. Note the markedly decreased global uptake in the affected individual. The bar chart summarizes the results from individuals 1.1, 2.3, 3.1, 3.2, and 4.1.; normal uptake is indicated by the horizontal dashed black line. (C) Patients had normal kidney histology. Shown is a representative image from a kidney biopsy of individual 1.1 stained with hematoxylin and eosin (H&E). Note the normal glomerular, tubular and interstitial morphology (scale bar 50 μ m). (D) Affected individuals had sensorineural deafness. Shown is a representative audiogram from affected individual 4.1 (solid line). Note the pronounced hearing loss for higher frequencies compared to control (dashed line).

Figure 2: Genetics

(A) Shown are the pedigrees of four families studied suggesting autosomal recessive inheritance. Females are represented by circles and males by squares. A double line between parents indicates consanguinity. Affected individuals are denoted by filled symbols. The numbers below these symbols denote individuals as referred to in the text. (B) The combined multipoint parametric linkage analysis shows a single genome wide significant peak on chromosome 11, with a maximum LOD score (y-axis) of 7.2. Genetic distance (in centimorgan) and individual chromosomes (1 to 22) are indicated on the lower and upper X-axes, respectively. (C) Representative sequence chromatograms. The EHD1 variant c.1192C>T (indicated by an arrow) is homozygous in an affected individual (left upper panel), absent in the reference sequence (right upper panel) and heterozygous in both parents (lower panels). (D) Regional homology plot of the protein sequence of EHD1 around the change of amino acid 398 from arginine to tryptophan (indicated by arrow). Note the strict and complete evolutionary conservation of R398.

1
2
3 Figure 3: EHD1 localization and function in the kidney
4

5 (A) Localization of EHD1 (green) in the normal human proximal tubule. Please note strong EHD1 signal
6 in the subapical compartment beneath the tubular lumen. Nuclear staining (blue); scale bar 10 μm .
7
8 (B) Normal human kidney showing very little or absent expression of EHD1 (green) within the
9 glomerulus and EHD1 prominence in adjacent proximal tubules. Nuclear staining (blue); scale bar 50
10 μm . (C-E), Kidney sections showing reabsorption of fluorescently labeled β_2 -microglobulin (white) (30
11 min after injection) in proximal tubules in a wildtype (C), knockout (D) and knockin mouse (E). Note,
12 in wildtype mouse kidney (c) reabsorption of fluorescently labeled β_2 -microglobulin was observed
13 mainly in early proximal tubules (S1 and S2 segments). In kidneys of homozygous *Ehd1* knockout (D)
14 or *Ehd1*^{R398W/R398W} mice (E), reabsorption of β_2 -microglobulin was not complete after passage of
15 tubular fluid through the early portions of the proximal tubule. Therefore, reabsorption was also
16 observed in late proximal tubules and a spillover of β_2 -microglobulin into urine (F) was observed. Scale
17 bars 100 μm . (F) Summary of urinary excretion of labeled β_2 -microglobulin during 30 min. Please note
18 the increased urinary loss in homozygous *Ehd1* knockout (KO) and knockin (R398W) mice. Asterisks
19 indicate $p \leq 0.05$ (ANOVA with Dunnett's multiple comparison test). (G) Summary of intravital
20 multiphoton microscopy revealing decreased reabsorption of fluorescently labeled β_2 -microglobulin
21 (10 min after injection) into proximal tubules of *Ehd1* knockout mice (symbols indicate individual
22 tubules, 6 animals each group). Asterisk indicates $p \leq 0.05$ (t-test).
23
24
25
26
27
28
29
30
31
32
33
34
35
36
37

38 Figure 4: EHD1 localization in relation to Cubilin and Megalin
39

40 In wildtype mice (upper row), *Ehd1* (green) was predominantly localized in the subapical
41 compartment. Cubilin is shown in red, Megalin in blue, cell nuclei (DAPI) in magenta. In knockout mice
42 (middle row) and knockin mice (lower row), the localization of Cubilin and Megalin appeared
43 unaffected. In knockin mice, *Ehd1* abundance was reduced and mutant *Ehd1* was observed in
44 intracellular tubules. Left four panels are confocal images; right high magnification panel: STED image
45 for *Ehd1*, Cubilin, and Megalin. Deconvolution of all images was performed using Huygens software.
46
47
48
49
50 Scale bar: 5 μm .
51
52
53
54
55
56
57
58
59
60

1
2
3 Figure 5: Ehd1 and inner ear
4

5 (A) Localization of Ehd1 (green) in stria vascularis (inner ear). In wildtype mice, Ehd1 was strongly
6 expressed in the stria vascularis (SV). In homozygous knockout (B) and knockin mice (C) the labeling
7 of stria vascularis (SV) and Reissner membrane (RM) was absent or grossly diminished, respectively.
8 (SM) scala media (containing endolymph); scale bar 50 μ m. (D) Auditory brainstem response
9 measurements of mice revealed a high-frequency hearing impairment in homozygous knockin mice
10 (*Ehd1*^{R398W/R398W}, n=6, red symbols) compared to wildtype mice (*Ehd1*^{wt/wt}, n=7, black symbols). Please
11 note the reverse scaling of the y-axis to facilitate comparison with the hearing phenotype of the
12 patient shown in Figure 1. Asterisks indicates $p \leq 0.05$ between groups (t-test with Bonferroni-Dunn
13 correction for multiple testing).
14
15
16
17
18
19
20
21
22
23
24

25 Figure 6: Cellular consequences of mutant EHD1 and protein stability
26

27 (A) Immunostained human EHD1 in inducible porcine proximal tubular cells (LLC-PK1). Please note the
28 “spotty” pattern in cells expressing wildtype EHD1 (left panel) and long intracellular structures,
29 presumably tubular recycling endosomes, decorated with EHD1^{R398W}. (B) Western blot of cell lysates
30 after removal of tetracycline that was used to induce expression of wildtype or mutant EHD1. Please
31 note the faster decay of EHD1 protein in cells expressing mutant EHD1. (C) Summary of experiments
32 as depicted in (B). EHD1-WT (white bars, filled black symbols), EHD1^{R398} (gray bars, open symbols).
33 Error bars indicate SEM, asterisks $p \leq 0.05$.
34
35
36
37
38
39
40
41
42

43 Figure 7: Structural consequences and cell model
44

45 (A) Three copies of the activated EHD1 homology model were arranged as oligomer similar to the
46 packing of EHD4 in the crystal (pdb entry code 4CDI). A potential arrangement of the EHD1 oligomer
47 (here trimer of dimers) at the membrane is visualized. The KPF loop (colored in yellow) of one dimer
48 facilitates major dimer-dimer contacts allowing for a repetitive back-to-front arrangement of EHD1
49 dimers. (B) Homology modelling suggested that Arg398 located at the tip of α_{12} faces towards the
50 dimer-interface. A possible interaction that would contribute to the dimer-interactions is Glu106-
51 Arg398, which would further stabilize the interaction of the KPF loop (Pro110-Arg135) with α_{12} . (C)
52 Side-on view of oligomeric form of EHD4. Membrane binding is predicted to be at the bottom. The
53 arrow indicates the position of the mutated residue at equivalent position 398 in EHD1. (D) Zoomed
54
55
56
57
58
59
60

1
2
3 view of the tryptophan (W) at the equivalent position 398 in human EHD1. The W is shown in stick
4 representation, projecting close to a loop of the nucleotide-binding pocket. ATP γ S is shown bound in
5 this pocket in space filling representation. Note the close proximity of the W residue, which is likely to
6 constrain nucleotide binding, hydrolysis or release by EHD1.
7
8
9

10 (E) Simplified model of endocytosis and recycling of membranes and receptors in normal proximal
11 tubules. (1) At the base of the brush border membrane, after Megalin and Cubilin (not shown) bind
12 their ligands, such as filtered proteins, the plasma membrane forms invaginations, mostly via Clathrin-
13 coated pits, which lead to the formation of endosomes (2). The endosomes are further processed into
14 sorting endosomes (3) and the endocytic recycling compartment (SE/ERC). Low pH in vacuoles
15 contributes to the separation of ligands from their receptors (4). From the endocytic
16 vacuoles/recycling endosomes, these dissociated ligands are directed to multivesicular bodies (not
17 shown) and finally to lysosomes. Receptor-containing vesicles are redirected to the apical membrane
18 (via dense apical tubules). EHD1 and its dimers/oligomers are involved in fission of the endocytic
19 tubules (5) and support receptor recycling (6). (F) Tubule fission is impaired in EHD1 patients and
20 knockin mice. Mutant EHD1 dysfunction slows the recycling rate and leads to renal tubular
21 proteinuria, as demonstrated in affected individuals and in animal models. In addition, mutant EHD1
22 forms aggregates in the cytosol. Megalin and Cubilin are not found in these aggregates, suggesting
23 that EHD1 does not physically interact with these receptor proteins.
24
25
26
27
28
29
30
31
32
33
34
35
36
37
38
39
40
41
42
43
44
45
46
47
48
49
50
51
52
53
54
55
56
57
58
59
60

1
2
3
4
5
6
7
8
9
10
11
12
13
14
15
16
17
18
19
20
21
22
23
24
25
26
27
28
29
30
31
32
33
34
35
36
37
38
39
40
41
42
43
44
45
46
47
48
49
50
51
52
53
54
55
56
57
58
59
60

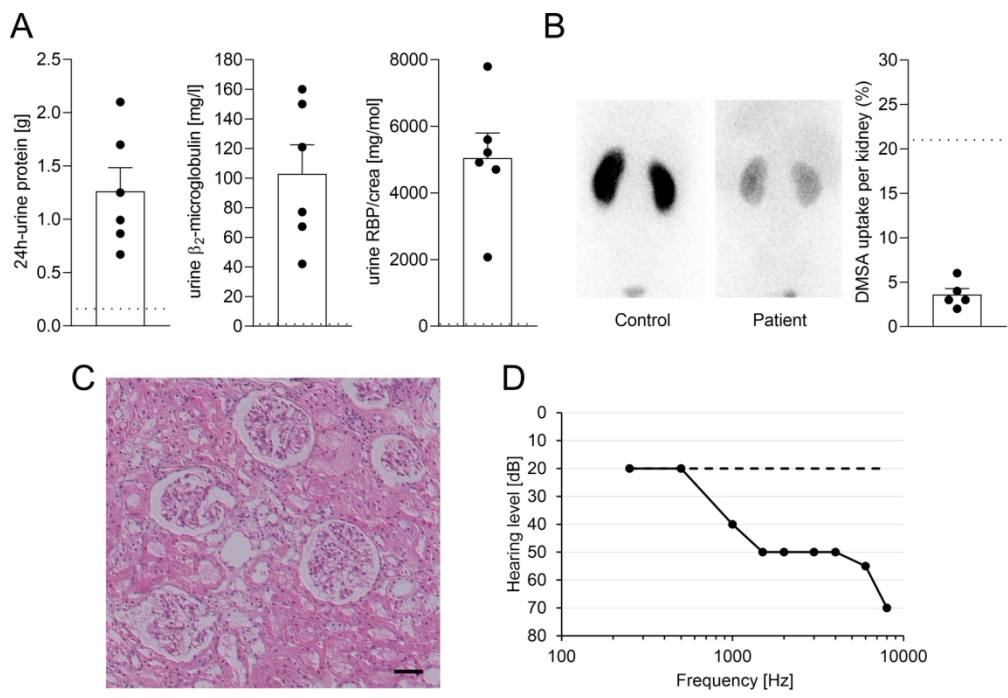


Figure 1: Human phenotype
149x101mm (300 x 300 DPI)

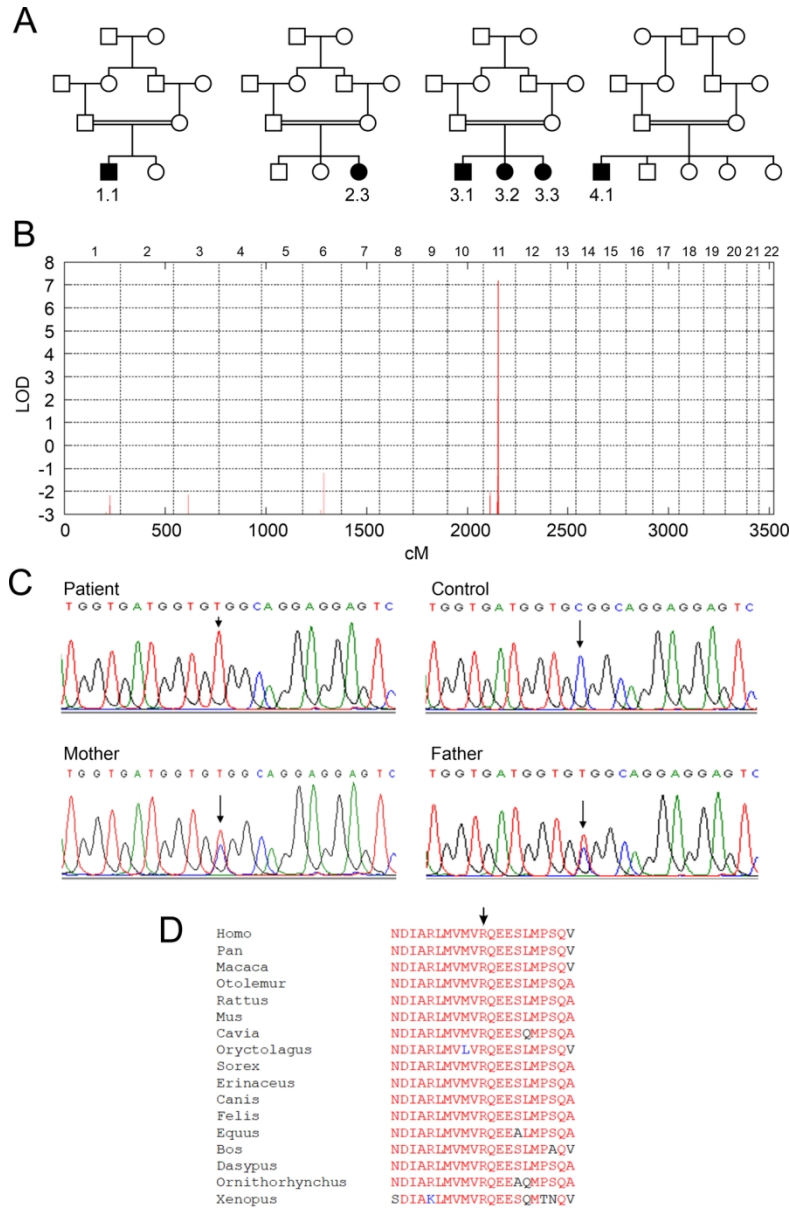


Figure 2: Genetics

119x183mm (300 x 300 DPI)

1
2
3
4
5
6
7
8
9
10
11
12
13
14
15
16
17
18
19
20
21
22
23
24
25
26
27
28
29
30
31
32
33
34
35
36
37
38
39
40
41
42
43
44
45
46
47
48
49
50
51
52
53
54
55
56
57
58
59
60

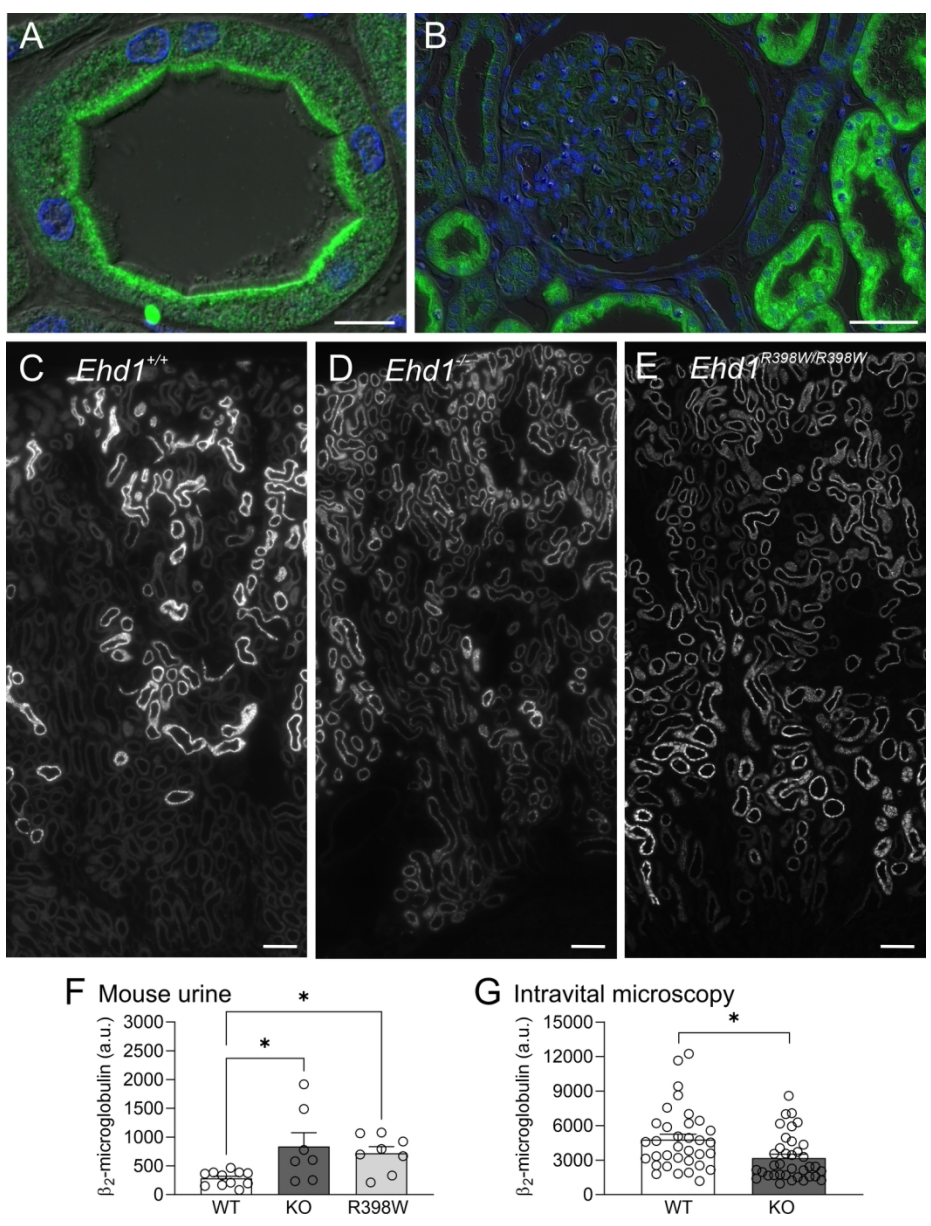


Figure 3: EHD1 localization and function in the kidney

138x180mm (300 x 300 DPI)

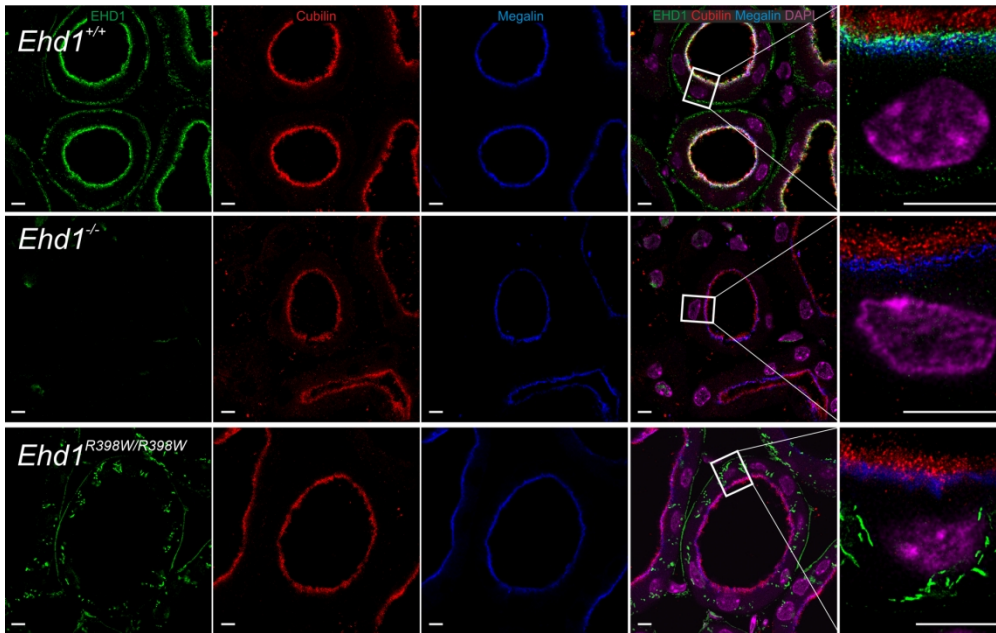


Figure 4: EHD1 localization in relation to Cubilin and Megalin

169x106mm (300 x 300 DPI)

1
2
3
4
5
6
7
8
9
10
11
12
13
14
15
16
17
18
19
20
21
22
23
24
25
26
27
28
29
30
31
32
33
34
35
36
37
38
39
40
41
42
43
44
45
46
47
48
49
50
51
52
53
54
55
56
57
58
59
60

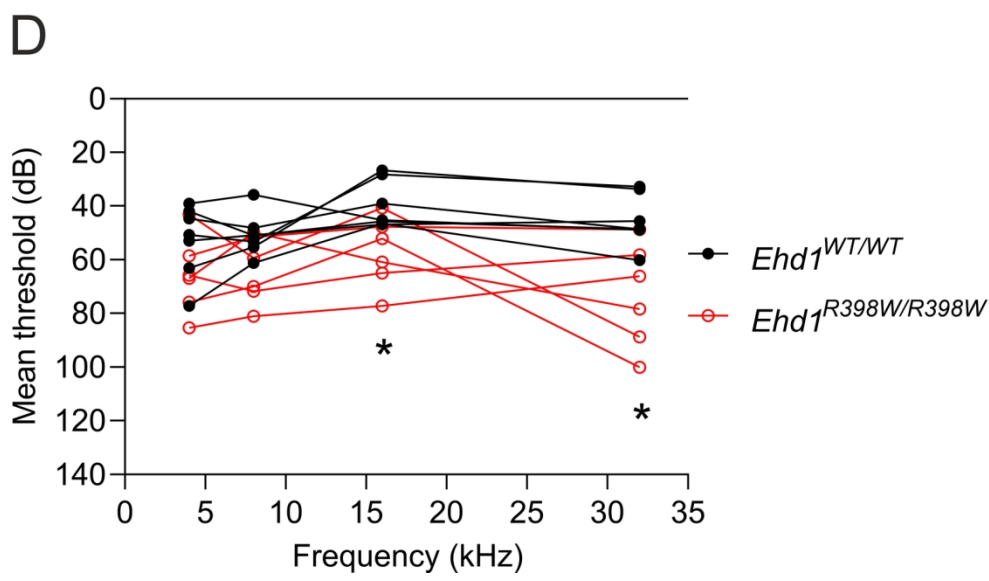
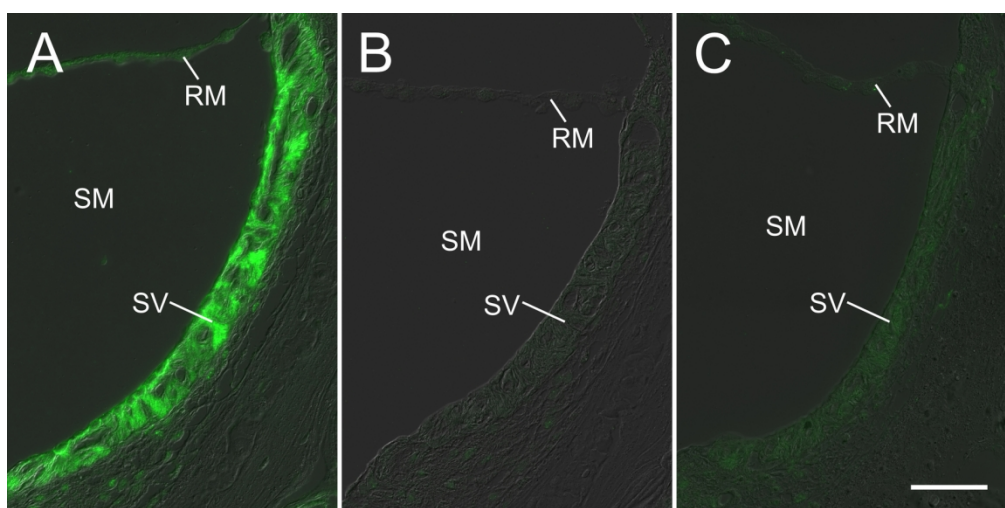


Figure 5: Ehd1 and inner ear
153x168mm (300 x 300 DPI)

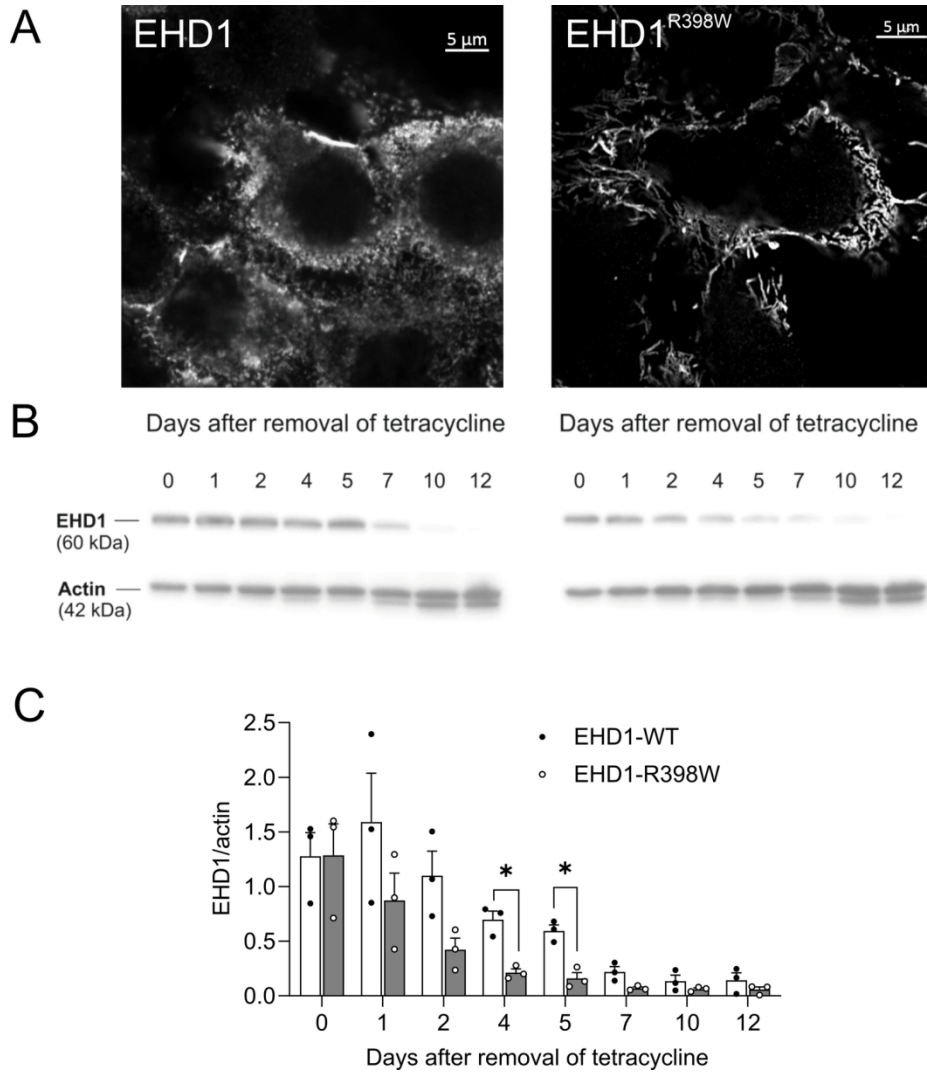


Figure 6: Cellular consequences of mutant EHD1 and protein stability

146x155mm (300 x 300 DPI)

1
2
3
4
5
6
7
8
9
10
11
12
13
14
15
16
17
18
19
20
21
22
23
24
25
26
27
28
29
30
31
32
33
34
35
36
37
38
39
40
41
42
43
44
45
46
47
48
49
50
51
52
53
54
55
56
57
58
59
60

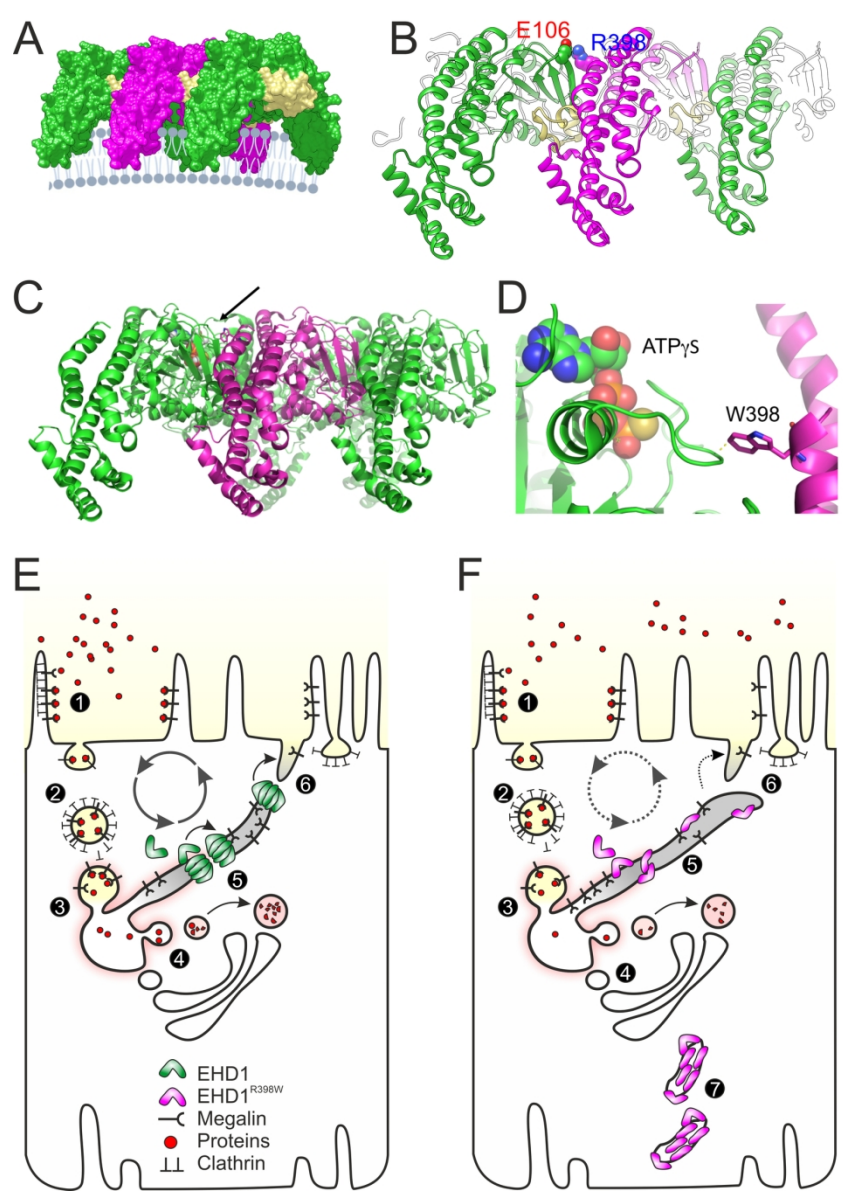


Figure 7: Structural consequences and cell model

140x199mm (300 x 300 DPI)

Supplement

A founder mutation in EHD1 presents with tubular proteinuria and deafness

Naomi Issler ^{1#}, Sara Afonso ^{2#}, Irith Weissman ^{3#}, Katrin Jordan ², Alberto Cebrian-Serrano ⁴, Katrin Meindl ², Eileen Dahlke ⁵, Konstantin Tziridis ⁶, Guanhua Yan ⁷, José M. Robles-López ⁷, Lydia Tabernero ⁷, Vaksha Patel ¹, Anne Kesselheim ¹, Enriko D. Klootwijk ¹, Horia C. Stanescu ¹, Simona Dumitriu ¹, Daniela Iancu ¹, Mehmet Tekman ¹, Monika Mozere ¹, Graciana Jaureguiberry ¹, Priya Outtandy ¹, Claire Russell ⁷, Anna-Lena Forst ², Christina Sterner ², Elena-Sofia Heintz ², Helga Othmen ², Ines Tegtmeier ², Markus Reichold ², Ina Maria Schiessl ⁹, Katharina Limm ¹⁰, Peter Oefner ¹⁰, Ralph Witzgall ¹¹, Lifei Fu ¹², Franziska Theilig ⁵, Achim Schilling ⁶, Efrat Shuster Biton ³, Limor Kalfon ³, Ayalla Fedida ³, Elite Arnon-Sheleg ³, Ofer Ben Izhak ¹³, Daniella Magen ¹³, Yair Anikster ¹⁴, Holger Schulze ⁶, Christine Ziegler ¹², Martin Lowe ⁷, Benjamin Davies ⁴, Detlef Böckenhauer ¹, Robert Kleta ^{1*#}, Tzipora C. Falik Zaccai ^{3#}, Richard Warth ^{2*#}

contributed equally

¹ Department of Renal Medicine, UCL, London, UK

² Medical Cell Biology, University Regensburg, Germany

³ Galilee Medical Center, Nahariya, Israel

⁴ Wellcome Centre Human Genetics, University Oxford, UK

⁵ Institute of Anatomy, University Kiel, Germany

⁶ ENT Clinic, University Hospital Erlangen, Germany

⁷ Division of Molecular & Cellular Function, University Manchester, UK

⁸ Royal Veterinary College, London, UK

⁹ Institute of Physiology, University Regensburg, Germany

¹⁰ Institute of Functional Genomics, University Regensburg, Germany

¹¹ Molecular and Cellular Anatomy, University Regensburg, Germany

¹² Structural Biology, University Regensburg, Germany

¹³ Pediatric Nephrology Institute, Haifa, Israel

¹⁴ Sheba Medical Center, Tel-Aviv, Israel

*Corresponding authors:

Robert Kleta, MD/PhD
Potter Chair of Nephrology
Department of Renal Medicine
University College London
Rowland Hill Street, London NW3 2PF, UK
phone: ++44-20 7314 7554
email: r.kleta@ucl.ac.uk

Richard Warth, MD
Medical Cell Biology
University Regensburg
Universitaetsstr. 31, 93053 Regensburg,
Germany
phone: ++49 941 943 2894
email: richard.warth@ur.de

1
2
3 **Contents**
4

5 Supplemental Methods 3
6
7 *Ehd1* knockout mice 3
8 *Ehd1*^{R398W/R398W} knockin mice 3
9
10 Immunostaining..... 3
11 Stimulated-Emission–Depletion (STED) super-resolution microscopy 4
12 Fluorescent labeling of β_2 -microglobulin..... 5
13 Reabsorption of β_2 -microglobulin..... 5
14 RNAScope of kidneys..... 5
15 Auditory brainstem response measurement..... 6
16 Intravital microscopy of renal proximal tubular endocytosis 6
17 Zebrafish strains and husbandry 7
18 Zebrafish RNA isolation, RT-PCR and Q-PCR..... 7
19 Morpholino injections into zebrafish 7
20 Injection and analysis of endocytic tracer..... 7
21 Western blotting of zebrafish larvae 8
22 Ethics statement on Zebrafish experiments 8
23 Proteomics..... 8
24 Homology modelling of EHD1 and EHD1^{R398W} 9
25 Statistics..... 10
26 Supplemental Tables 11
27 Supplemental Table 1: Clinical phenotype details..... 11
28 Supplemental Table 2: Breeding statistics 12
29 Supplemental Figures 13
30 Supplemental Figure 1: EHD1 in human kidney..... 13
31 Supplemental Figure 2: Ehd1 in mouse kidney 14
32 Supplemental Figure 3: Localization Ehd1, Megalin and reabsorbed β_2 -microglobulin 15
33 Supplemental Figure 4. Zebrafish..... 16
34 Supplemental Figure 5: Localization of Ehd1^{R398W} in mouse kidney 17
35 Supplemental Figure 6: Localization of Ehd1 and Arf6 in mouse kidneys 18
36 Supplemental Figure 7: Effect of *Ehd1* knockout and knockin on the localization of Rab11 19
37 Supplemental Figure 8: Intravital multiphoton microscopy 20
38 Supplemental Figure 9: EHD1 and MICAL-L1 in EDH1-overexpressing LLC-PK1 cells 21
39 Supplemental Figure 10: MICAL-L1 and Pacsin 2 in cells overexpressing EDH1^{R398W} 22
40 Supplemental Figure 11: Primary cilia in murine and human kidneys..... 23
41 Supplemental Figure 12: Alignment of EHD1, EHD2 and EHD4 24
42 Supplemental Figure 13: Structural modeling: Putative structure of EHD1 dimers..... 25
43 Supplemental Figure 14: Structural modeling: Effects of the R398W mutation on EHD1
44 oligomerization..... 26
45 Supplemental References..... 27
46
47
48
49
50
51
52
53
54
55
56
57
58
59
60

Supplemental Methods

***Ehd1* knockout mice**

Experiments were performed according to the guidelines for the care and use of laboratory animals published by the US National Institutes of Health and were approved by the local councils for animal care according to the German law for animal care. Animal experiments on mice to assess renal function were approved by the Regierung Unterfranken, Germany.

We thank the Wellcome Trust Sanger Institute Mouse Genetics Project (Sanger MGP) and its funders for providing the mutant mouse line C57BL/6NTac-*Ehd1*^{tm1a(EUCOMM)Wtsi/WtsiBiat} ([https://www.mousephenotype.org/data/alleles/MGI:1341878/tm1a\(EUCOMM\)Wtsi](https://www.mousephenotype.org/data/alleles/MGI:1341878/tm1a(EUCOMM)Wtsi)), and the European Mouse Mutant Archive (<https://www.infrafrontier.eu>; EMMA ID: EM:05712) from which the mouse line was received. These mice carrying a floxed exon 2 of *Ehd1* were bred with a global 129/Sv Cre Recombinase pCX-NLS Cre mouse. In the offspring deletion of exon 2 was confirmed and mice were crossed to obtain homozygous progeny for the *Ehd1* gene deletion (*Ehd1*^{-/-}).

***Ehd1*^{R398W/R398W} knockin mice**

The *Ehd1* knockin mice were generated in house (Wellcome Centre for Human Genetics, University of Oxford, United Kingdom) using Crispr/Cas9 technologies. A CRISPR/Cas9 nuclease was designed against the sequence 5'-GATGGTGATGGTGCGCCAGG-3' within exon 5 (ENSMUSE00000232103) of the mouse *Ehd1* gene, the target site of which encompasses the Arginine-398 residue which we identified to be mutated to a Tryptophan residue in families with hereditary tubular proteinuria and hearing deficit. A single stranded oligonucleotide harboring the desired point mutation was designed and used as a template for homology directed repair to introduce the orthologous mutation into the mouse genome. The single-strand oligodeoxynucleotide (ssODN) and the guide-RNA, prepared by in vitro transcription, for the designed CRISPR/Cas9 nuclease were microinjected into fertilized C57BL/6J oocytes prepared from transgenic female mice that overexpress Cas9¹. In the resulting litters, multiple founder mice were generated which harbored the desired R398W mutation. The production of the knockin mice was carried out in accordance with UK Home Office Animal [Scientific Procedures] Act 1986, with procedures reviewed by the Clinical Medicine Animal Welfare and Ethical Review Board at the University of Oxford, and conducted under project license PPL 30/3085.

Immunostaining

Mice were sacrificed by exsanguination in deep anesthesia (2.5% isoflurane). Immediately post mortem, the animals were perfused via the abdominal aorta with 3% paraformaldehyde dissolved in a solution of 100 mM sucrose, 90 mM NaCl, 15 mM K₂HPO₄, 1 mM EGTA and 2 mM MgCl₂ (pH 7.4). The fixed kidneys were removed and either frozen in liquid nitrogen for cryo-sectioning or further processed for standard paraffin embedding.

For immunofluorescence staining on paraffin-embedded tissue, the sections were deparaffinized and epitope unmasking was performed by incubation in citrate buffer (pH 6.0) at 95°C for 15 min. On cryo-sections epitope unmasking was performed by incubation in 0.1% SDS solution for 5 min. Unspecific

antibody binding sites were blocked using 5% BSA solution for 10 min. Primary and secondary antibodies were diluted in PBS based solution containing 0.5% BSA and 0.04% Triton X-100. Primary antibody incubation was performed overnight at 4°C. Tissue sections were washed with PBS before adding the secondary antibody for 1 h at room temperature. Sections were mounted using DAKO glycergel mounting medium (Agilent). Immunofluorescence signals of stained sections were analyzed using an inverted microscope (Axiovert 200, Zeiss) or a confocal microscope (LSM 710, Zeiss).

Stimulated-Emission-Depletion (STED) super-resolution microscopy

For STED microscopy, Cryosections for Rab11A staining were antigen retrieved using 0.5% tritonX-100 in PBS. Paraffin sections were used for triple-antibody staining of EHD1/Cubilin/Megalín. Heat-induced antigen retrieval were performed in citrate buffer (pH 6). Sections were blocked with 10% donkey serum/PBS and sequentially incubated with primary antibodies in 5% donkey serum/PBS overnight. Suitable StarRed-, Star580-, Alexa488-coupled secondary antibodies (Abberior, Göttingen, Germany; Dianova, Hamburg, Germany) were used. Counter staining were performed using Acti-stain 488 Phalloidin (Cytoskeleton) and/or 4',6-diamidino-2-phenylindole. Sections were mounted with Abberior Liquid Mount and analyzed using a multilaser confocal scanning microscope and/or stimulated-emission-depletion super-resolution microscopy (see below).

Images were acquired using Facility Line (Abberior Instruments, Göttingen, Germany) with Olympus IX83 microscope (Germany) and Inspector software (Abberior Instruments) in confocal microscopy mode or STED mode. The images were de-convolved using Huygens Professional Software (version 20.10, Scientific Volume Imaging B.V., Netherlands). The Classic Maximum Likelihood Estimation (CMLE) algorithm for deconvolution was performed using standard setting (quality change threshold 0.1%).

Antibody/substance	Type	Dilution for immuno-fluorescence	Producer
anti-ARL13B, rabbit polyclonal IgG	Prim.-Ab	1:500	Proteintech Germany, St. Leon-Rot, Germany
anti-EHD1, rabbit monoclonal [EPR4954] IgG	Prim.-Ab	1:200	Abcam, Cambridge, UK
anti-EHD1 for Supplemental Figure 12	Prim.-Ab	1:200	Kind gift from S. Caplan, University of Nebraska
Anti-Aquaporin-2 (C17), goat polyclonal antibody	Prim.-Ab	1:500	Santa Cruz, Heidelberg, Germany
Anti-Megalín, guinea pig polyclonal antibody	Prim.-Ab	1:1000	F. Theilig, University of Kiel ²
Anti-MICAL-L1, guinea pig polyclonal antibody, H00085377 B01P	Prim.-Ab	1:200	Abnova
anti-Rab11A, rabbit polyclonal antibody	Prim.-Ab	1:100	Invitrogen
anti-Cubilín (T-16), goat polyclonal antibody	Prim.-Ab	1:30	Santa Cruz
anti-Arf6, mouse monoclonal	Prim.-Ab	1:100	Kind gift from J. Barhanin ³
anti-acetylated tubulin, mouse monoclonal, (T6793)	Prim.-Ab	1:100	Sigma Aldrich

StarRED donkey anti-rabbit	Sec.-Ab	1:50	Abberior; Dianova, Hamburg, Germany
Star580 donkey anti-rabbit	Sec.-Ab	1:50	Abberior; Dianova, Hamburg, Germany
Star580 donkey anti-mouse	Sec.-Ab	1:50	Abberior; Dianova, Hamburg, Germany
Alexa Fluor® 488 donkey anti-goat	Sec.-Ab	1:50	Dianova, Hamburg, Germany
Acti-stain 488 Phalloidin	Actin Stain	1:200	Cytoskeleton, Denver, USA
Alexa Fluor® 488 donkey anti-rabbit	Sec.-Ab	1:400	Thermo Fisher Scientific, Dreieich, Germany
Alexa Fluor® 555 donkey anti-rabbit	Sec.-Ab	1:400	Thermo Fisher Scientific, Dreieich, Germany
Alexa Fluor® 555 donkey anti-goat	Sec.-Ab	1:400	Invitrogen, Karlsruhe, Germany
Alexa Fluor® 647 donkey anti-guinea-pig	Sec.-Ab	1:400	Invitrogen, Karlsruhe, Germany
HOE33342 (5x10 ⁻² M)	Nuclear stain	1:400	Invitrogen, Karlsruhe, Germany
DAPI	Nuclear stain	1:2000	Thermo Fischer

Fluorescent labeling of β_2 -microglobulin

1 mg protein of recombinant, human β_2 -microglobulin expressed in *E. coli* (Merck) was used for conjugation with the fluorescent tag Alexa Fluor™ 546 using the Alexa Fluor™ 546 Protein Labelling Kit (Thermo Fisher) according to the manufacturer's instructions. The conjugates were separated from the unconjugated dye by exclusion purification resin. The obtained β_2 -microglobulin-Alexa Fluor 546 conjugate had a concentration of ~750 μ M.

Reabsorption of β_2 -microglobulin

To assess renal reabsorption of β_2 -microglobulin, age-matched mice were anesthetized using isoflurane inhalation (1.5% isoflurane in a gas mixture of 50% oxygen and 50% nitrogen). A catheter was placed into the femoral vein, the bladder was emptied and a 1:50 dilution (in 0.9% NaCl) of the above-mentioned Alexa Fluor 546 labeled β_2 -microglobulin was injected into the femoral vein at a dose of 20 μ l/g body weight. 30 min later, urine and blood were collected and the mice were sacrificed by exsanguination via the vena cava. Immediately post mortem, animals were perfused with fixative via the abdominal aorta. Both kidneys were harvested; one was homogenized in distilled water, the other one was prepared for cryo-sectioning. The fluorescence intensity of Alexa Fluor 546 in plasma, urine and kidney homogenate was measured using a microplate reader (NOVOstar microplate reader).

RNAScope of kidneys

RNAScope experiments were performed on paraffin-embedded kidneys using the RNAScope® 2.5 HD Assay Kit (ACD) according to the manufacturer's instructions.

Auditory brainstem response measurement

Animals aged between 6-8 weeks were used for the measurement of the auditory brainstem response. Mice were anaesthetized using a mixture of ketamine (96 mg/kg), xylazine (4 mg/kg) and physiological NaCl solution at a mixing ratio of 9:1:8, initial dose: 0,3 mL s.c.. Mice were placed within a sound-attenuated chamber on a thermally controlled heating pad at 37°C, and frequency-specific auditory brainstem responses (f-ABR) were measured. The protocol was performed as previously described⁴. Briefly, f-ABR were measured via subcutaneously placed thin silver wire electrodes (0.25 mm diameter) using a low noise amplifier (JHM NeuroAmp 401, J. Helbig Messtechnik, Mainaschaff, Germany; amplification 10,000; bandpass filter 400 to 2,000 Hz and 50 Hz notch filter) in combination with a custom-made Python program (Python 2.6) for stimulation and data recording. Auditory stimuli of 4, 8, 16 and 32 kHz were presented free-field to one ear at 3 cm distance from the animal's pinna via a custom-made speaker. The speaker's frequency response function was corrected to be flat within ± 1 dB. Stimuli presented were pure tones (6 ms duration including 2 ms cosine-squared rise and fall times) between the range of 1 and 32 kHz. 300 stimuli were presented with alternating inverted phase with a repetition rate of 4 Hz. The stimuli of all tested frequencies were presented pseudorandomized with different sound pressure levels between 30 dB and 100 dB with a step width of 5 dB. To obtain the f-ABR-based hearing thresholds, the mean sound intensity dependent f-ABR wave root-mean-square values independent for each frequency were fitted by hard-sigmoid functions. Thresholds were defined automatically by a custom-made Python program at the inflection point of that hard sigmoid fit. Variance of the calculated ABR thresholds were obtained by data subsampling. Data were discarded at frequencies where this procedure was not possible, for example, at very low signal-to-noise ratios. The statistical analysis of the individual and group threshold data was performed in Origin.

Intravital microscopy of renal proximal tubular endocytosis

Mice were anesthetized through inhalation of isoflurane (1.5-2.5% isoflurane). The body temperature was maintained at 37°C by placing the animals on an operating table with a servo-controlled heating plate. A cannula connected to a syringe was inserted into the right jugular for the intravenous infusion of the dyes. For kidney imaging, the left kidney was exposed by making a small flank incision. The experiments were performed using a Zeiss LSM 710 confocal fluorescence microscope. Excitation was achieved using a Chameleon Ultra-II MP laser (Coherent Deutschland, Dieburg, Germany) at 940 nm with a laser power of 20% of 3200 mW. Eight-bit 1454 x 1454 pixel images (providing a theoretical dynamic range for intensities measurements of 0–65536 pixel intensity) were obtained using a pixel dwell time of 3.15 μ s and a line average of one by applying a 40x long distance (LD) C- Apochromat 40/1.1 water objective. The emissions were collected using external detectors: Nondescanned detectors with filter set 1 (green channel): beam splitter 500–550 and long pass (LP) 555 and filter set 2 (red channel): beam splitter P 565–610 including mirror. The detector settings were kept constant for all measurements: for the green and red channels, respectively, the master gain was 600/600, the digital gain was 10/10, and the offset was -0.0/0.0. To label the vasculature, a 25 mg/ml solution of FITC-500 kDa Dextran conjugate dissolved in PBS was first concentrated using Nanosep Centrifugal (VWR International, Darmstadt, Germany) and injected intravenously (0.37 μ l/g body weight). The

1
2
3 fluorescence was detected using the green channel. After 1 min, the Alexa Fluor 546-labeled β_2 -
4 microglobulin dissolved in PBS was injected intravenously (1.56 μ l/g body weight) and the proximal
5 tubular β_2 -microglobulin uptake was measured as the increase in the tubular fluorescence intensity
6 during the 30 min after injection. The fluorescence was detected using the red channel. The mean
7 fluorescence intensity of Alexa Fluor 546-labeled β_2 -microglobulin measured in 3–6 proximal tubules
8 per animal over time (30 min, 15 images) and the background readings for the proximal tubular
9 autofluorescence before labeled β_2 -microglobulin injection were assessed using ImageJ V1.37c. The
10 reabsorption capacity of the proximal tubules was compared after 2, 4, 10, 20 and 30 min of β_2 -
11 microglobulin injection by assessing the mean fluorescence intensity of β_2 -microglobulin per tubule and
12 subtracting the background fluorescence.
13
14
15
16
17
18

19 **Zebrafish strains and husbandry**

20 Zebrafish were raised and maintained at the University of Manchester Biological Services Unit
21 according to the UK Animals Act 1986. The wildtype line was of the AB background.
22
23
24

25 **Zebrafish RNA isolation, RT-PCR and Q-PCR**

26 Total RNA was isolated from zebrafish embryos using Trizol (Invitrogen) and reverse-transcribed with
27 Superscript First Strand (Invitrogen) to produce cDNA. For direct visualization of amplification products,
28 cDNA was amplified using standard PCR conditions and appropriate primer pairs. Q-PCR was
29 performed using SYBR Green (Sigma-Aldrich) according to the manufacturer's protocol. 0.5 μ l cDNA
30 template from a 20 μ l aliquot generated from 5 μ g of RNA was used per reaction. Each experiment was
31 run in duplicate and was repeated on three individually obtained RNA extracts. Studies were performed
32 using the ABI PRISM 7000 sequence detector system (Applied Biosystems Ltd).
33
34
35
36
37

38 **Morpholino injections into zebrafish**

39 Morpholinos were obtained from GeneTools. The standard control morpholino had the sequence
40 CCTCTTACCTCAGTTACAATTTATA ([https://www.gene-tools.com/content/negative-control-](https://www.gene-tools.com/content/negative-control-morpholino-oligos)
41 [morpholino-oligos](https://www.gene-tools.com/content/negative-control-morpholino-oligos)). Morpholinos targeting zebrafish *ehd1* were the same as described previously, with
42 the following sequences: *ehd1a* (CTGAACATGGTGGACGTTACACGAC); *ehd1b*
43 (ATCTTTGTTAGACCAACTGAACATT) and were injected with morpholino targeting p53 (1 nl of a 250
44 μ M stock) into one cell stage embryos as described previously^{5, 6}.
45
46
47
48
49

50 **Injection and analysis of endocytic tracer**

51 Lysine-fixable 10 kDa dextran labelled with Alexa 488 (Molecular Probes) was prepared in PBS at 2
52 μ g/ μ l final concentration, and 1 nl was injected into the larval circulatory system. Zebrafish larvae at 4
53 dpf were anesthetized with 0.2 mg/ml MS222 (Sigma) in chorion water, and tracer injected into the
54 common cardinal vein using a glass micropipette PLI-90 Pico-Injector (Harvard Apparatus). Pronephric
55 uptake was assessed at 2.5 h on whole mounts using a fluorescence dissecting stereomicroscope
56 (Leica MZ10F). Statistical analysis was performed using the Pearson's chi-squared test with Prism
57 software (Prism Software Corporation).
58
59
60

Western blotting of zebrafish larvae

Larvae were culled by anaesthetic overdose and 100 collected per condition in 1.5 mL Eppendorf tubes. Embryos were then triturated ~15 times in Ginzburg fish ringers' solution (110 mM NaCl, 3.5 mM KCl, 2.7 mM CaCl₂·2H₂O, 10 mM Tris pH 8.5) containing 0.75 mM EDTA, 0.3 mM PMSF, and 20x protease inhibitor cocktail to remove the yolk sac. Larvae were centrifuged at 1800 rpm for 1 min, supernatant removed, and washed again in Ginzburg solution before analysis by Western blotting with antibodies to EHD1 (Steve Caplan, University of Nebraska) and GAPDH (Santa Cruz SC-25778).

Ethics statement on Zebrafish experiments

All work was performed under the UK Home Office animal project license number 70/9091. Local animal care was provided by the University of Manchester BSF Unit. Zebrafish larvae at 4 dpf were anesthetized with 0.2 mg/ml MS222 for injection of endocytic tracer. Following the experiment, euthanasia was performed by incubation in 0.2 mg/ml MS222 for >2h.

Proteomics

Mouse kidney was transferred to 2-ml Precellys tubes (Precellys® Keramik-Kit 1.4/2.8 mm, Bertin). Homogenisation was performed twice at 6,500 rpm for 20 sec in 1 ml of ice cold 80% MeOH by means of the Precellys® 24 Homogenisator (Bertin). Samples were then incubated at -20 °C overnight prior to centrifugation at 20,000 x g for 15 min at 4°C. Supernatant was discarded and the pellets were air-dried. Further lysis was performed in 1 ml of gel-aided sample preparation (GASP)-buffer⁷ supplemented with 20 mM DTT. Total protein amount was determined using the SERVA Purple Protein Quantification Assay (SERVA Electrophoresis GmbH) according to the manufacturer's instructions. Fifty micrograms of protein lysate were then processed using the GASP protocol as described previously⁷. After tryptic digestion, the peptide extracts were redissolved in 25 µl of 5% formic acid. Microliquid chromatographic (microLC) separations of tryptic digests were performed on an Eksigent-LC 425 (AB Sciex) coupled to an AB Sciex TripleTOF 5600+ mass spectrometer⁸. The tryptic digests (5 µg each) were injected directly onto a 150 × 0.3 mm I.D. CSH-C18 column (particle size 1.7 µm, 120 Å, Waters) and peptides were separated at a column temperature of 40 °C using a 85-min linear acetonitrile gradient (3–40%) in 0.1% formic acid at flow-rate of 6 µL/min. Samples were injected once each for mass spectrometric (MS) analysis in data-dependent acquisition (DDA) mode and Sequential Window Acquisition of all THEoretical fragment-ion spectra (SWATH), respectively⁹. For peptide library generation, the TripleTOF 5600+ mass spectrometer (AB Sciex, Darmstadt, Germany) was operated in DDA mode from 400–1,000 m/z for 250 ms, followed by acquisition of MS/MS-spectra from 230–1,500 m/z of the 20 most intensive precursor ions for 50 ms per precursor. The data were searched using ProteinPilot 5.0 (AB Sciex) against the UniProtKB/Swiss-Prot (Version 03-2021) database. For SWATH-MS, an initial 50 ms TOF-MS full scan was employed, before the entire m/z range of 230–1,500 was covered using 60 SWATH variable windows of 50 ms each¹⁰. For quantification of the proteins from the SWATH runs the PeakView 2.2 software (AB Sciex) and the MicroApp 2.0.1 were used.

Homology modelling of EHD1 and EHD1^{R398W}

Human EHD isoforms EHD1, EHD2 and EHD4 exhibit high sequence identities of about 70% (Supplemental Figure 7). Two homology models of EHD1 were generated based on crystal structures of the autoinhibited state of EHD2 (pdb entry code 4CDI) (Supplemental Figure 8A and 8B) and the activated state of EHD4 (pdb entry code 5MTV) (Supplemental Figure 8C and 8D) as respective templates. Arg398 in both models is located at the very end of helix α 12 in front of the linker loop to the EH-domains pointing away from the dimer interface and the GTPase domain (Supplemental Figure 8B and 8D). At a first glance, a functional role for Arg398 and the phenotype seen in EHD1^{R398W} is not obvious from the homology models. However, looking into the activation mechanisms of EHD proteins points towards a problem in oligomerization as consequence of the R398W mutation found in our patients.

The auto-inhibited state differs from activated state in EHDs in the orientation of helix α 8, which rotates over 60° around a hinge point at Pro286 (Supplemental Figure 7, black star and Supplemental Figure 8). In the inhibited state, α 8 is wedged between the N-terminal helical domain α (1a,b) and a bundle of three small helices α 9 - α 11 (pink in Supplemental Figure 8B and 8D) which are known to be involved in membrane interactions. Activation is suggested to start with a conformational change of the N-terminal domain at the membrane surface, thereby releasing α 8, which snaps like a Swiss army knife into the extended conformation (Supplemental Figure 8C and 8D). This rigid-body movement is accompanied by several changes such as the detachment of the EH-domain from the GTPase domain, re-arrangement of the membrane interacting bundle α 9 - α 11 (Supplemental Figure 8B and 8D), and re-folding and relocation of the KPF loop. None of these conformational changes seem to involve Arg398, which rather faces away from the KPF loop within a monomer. However, in the active state EHD1 dimers oligomerize in a front-to-back orientation mediated by the KPF loop of individual dimers (Supplemental Figure 9A and 9B). In the context of this oligomerization Arg398 in EHD1 might provide a re-enforcement of dimer-dimer interaction. A likely partner candidate is Glu106 that is located just in front of the KPF loop of the adjacent dimer. A Glu106-Arg398 interaction (Supplemental Figure 9B) might help sculpturing the oligomerization interface further.

Ab initio mutation against tryptophan in the homology model of EHD1^{R398W} did not alter the overall conformation of the EHD1 dimer but the introduction of a bulky and hydrophobic residue like tryptophan would affect this most relevant oligomerization interface (Supplemental Figure 9C). In addition, Trp398 might form inter-monomer interaction, e.g., with Arg287, linking α 8 - α 12 together. Any change along the dimer-dimer interface will affect the interaction of the KPF loop with the membrane interacting helices (pink in Supplemental Figure 9C). We suggest that even subtle reorientations of the α 9 - α 11 bundle with respect to the membrane plane might alter the geometry of membrane fission and could cause the phenotypical change in membrane morphology in EHD1^{R398W}.

1
2
3 Another hypothesis explaining the functional deficit of the R398W mutant is based on the seminal works
4 of Daumke et al. ^{11, 12}. EHD1 and EHD4 (mouse EHD4 ADP conformation structure: pdb 5MVF; mouse
5 EHD4 ATP conformation structure: pdb 5MTV) are well conserved at the protein level, and the published
6 sequences of EHD2 (mouse EHD2 pdb 2QPT) and EHD4 are very similar, so we are confident the
7 modeling is accurate. According to our modeling, the mutated R398 of human EHD1 lies very close to
8 the nucleotide-binding pocket of an adjacent EHD1 protein within the EHD1 oligomer, based upon the
9 crystal packing structure (Supplemental Figure 10). The conversion of R398 to W would result in a likely
10 physical constraint of the loops constituting the nucleotide-binding pocket. This, we predict, would either
11 interfere with nucleotide binding, nucleotide hydrolysis, or release of nucleotide following catalysis. We
12 favor the last two based upon the cellular phenotype of the mutant, which is membrane-bound
13 (suggesting binding to ATP), and able to drive membrane tubulation consistent with a lack of membrane
14 fission (Supplemental Figure 11). This in fact is similar to the phenotype seen with ATPase-deficient
15 mutant T94A in EHD2 ¹¹ strongly arguing for this mechanism as at least a contributing mechanism.
16
17
18
19
20
21
22

23 **Statistics**

24 Data are shown in mean values \pm standard error of the mean (SEM); “n” stands for the number of
25 observations. Unpaired two-sided Student’s t-test and ANOVA with Tukey’s or Dunnett’s multiple
26 comparison tests were used to calculate significance between different groups or time series,
27 respectively. A p-value ≤ 0.05 was accepted to indicate statistical significance, which was identified by
28 an asterisk (*). Statistics were performed using Origin V94E (OriginLab Corporation), SPPSS and
29 GraphPad Prism software.
30
31
32
33
34
35
36
37
38
39
40
41
42
43
44
45
46
47
48
49
50
51
52
53
54
55
56
57
58
59
60

Supplemental Tables

Supplemental Table 1: Clinical phenotype details

Patient	Age at diagnosis [years]	Albumin / creatinine ratio [mg/g]	24-h urine protein [g]	β 2M [mg/l]	Plasma Creatinine [mg/dl]	DMSA Renal uptake left / right [%]	Audiogram
1.1	11	189	2.1	121	0.5	2 / 1	SND
2.3	10	ND	1.0	42	0.6	6 / 6	SND
3.1	5	155	1.7	160	0.8	3 / 3	SND
3.2	12	ND	1.3	67	0.7	4 / 6	SND
3.3	33	54	0.9	77	0.7	ND	SND
4.1	14	178	0.7	150	0.6	3 / 3	SND
normal		< 30	< 0.15	< 1.8	0.2-1.0*	> 21 / > 21	

Shown are pertinent clinical and biochemical data. Note proteinuria, which is predominantly low-molecular weight, as indicated by the elevated β ₂-microglobulin (β 2M).

Note also the very low uptake of ^{99m}Tc-dimercaptosuccinic acid (DMSA) by the kidneys in the five tested affected individuals. Renal scintigraphy was performed four hours after administering 0.5mCi/kg of DMSA intravenously. The images were acquired using a double-head scintillation gamma camera equipped with a low-energy-high-resolution collimator (Infinia, General Electric, Haifa, Israel). Posterior planar images in the supine position were acquired with a 256x256 matrix and zoom=1 until 250,000 counts were detected. Single photon emission computed tomography (SPECT) images were acquired with a 64x64 matrix, zoom=1, 120 projections 3° apart with 15 second/projection. Renal uptake was calculated using the method detailed by Groshar et al. (Quantitation of Renal Uptake of Technetium-99m DMSA Using SPECT. J Nucl Med. 1989;30:246-250). Kidney volumes and radioactive concentration measurements were calculated using a customized computer program. For each kidney the injected dose (ID) per cc (%ID/cc) was measured and multiplied by the kidney volume for the calculation of the total kidney uptake. The patient uptake values were compared to uptake values in a normal population.

Moreover, all patients have sensorineural deafness (SND).

*The creatinine reference is age dependent: at the age of the youngest participant (5 years) it would be 0.2-0.5 mg/dl, and of the oldest (a female): 0.7-1.0 mg/dl. Note that plasma creatinine values are in the normal range for all. ND: not done.

Supplemental Table 2: Breeding statistics

n	female	male	<i>Ehd1</i> ^{+/+} pups	<i>Ehd1</i> ^{+/-} pups	<i>Ehd1</i> ^{-/-} pups	<i>Ehd1</i> ^{R398W/R398W} pups	<i>Ehd1</i> ^{R398W/wt} pups	<i>Ehd1</i> ^{wt/wt} pups	total
6*	<i>Ehd1</i> ^{+/-}	<i>Ehd1</i> ^{+/-}	60 (28%)	132 (61.7%)	22 (10.3%)				214
1	<i>Ehd1</i> ^{-/-}	<i>Ehd1</i> ^{+/-}	0	4 (80.0%)	1 (20%)				5
3	<i>Ehd1</i> ^{+/+}	<i>Ehd1</i> ^{-/-}	0	0	0				0
5*	<i>Ehd1</i> ^{R398W/wt}	<i>Ehd1</i> ^{R398W/wt}				32 (19.2%)	88 (52.7%)	47 (28.1%)	167
2*	<i>Ehd1</i> ^{R398W/wt}	<i>Ehd1</i> ^{R398W/R398W}				0	0	0	0

n denotes the number of breeding pairs; some breeding pairs produced multiple litters (*).

Ehd1^{R398W/R398W}: Knockin mice homozygous for the *Ehd1* mutation R398W.

Ehd1^{R398W/wt}: Knockin mice heterozygous for the *Ehd1* mutation R398W.

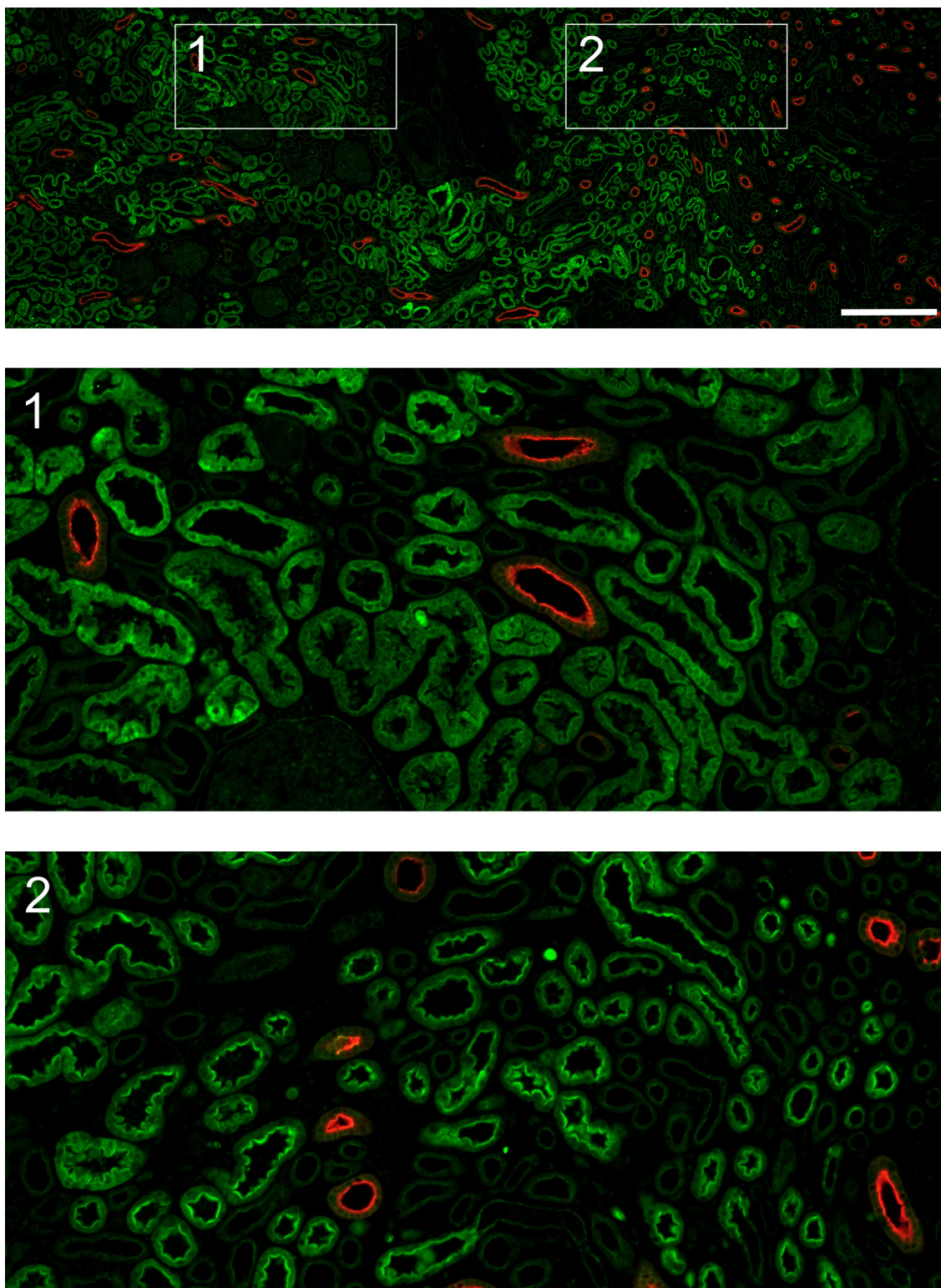
Ehd1^{wt/wt}: Littermates of knockin mice without the mutation R398W.

% was calculated for each genotype based on total genotyped pups for each breeding scheme.

Homozygous *Ehd1*^{-/-} and *Ehd1*^{R398W/R398W} male mice were bred for at least two months with at least one heterozygous or wildtype fertile female mouse. These breeding pairs produced no offspring indicating that male homozygous *Ehd1*^{-/-} and *Ehd1*^{R398W/R398W} mice were infertile.

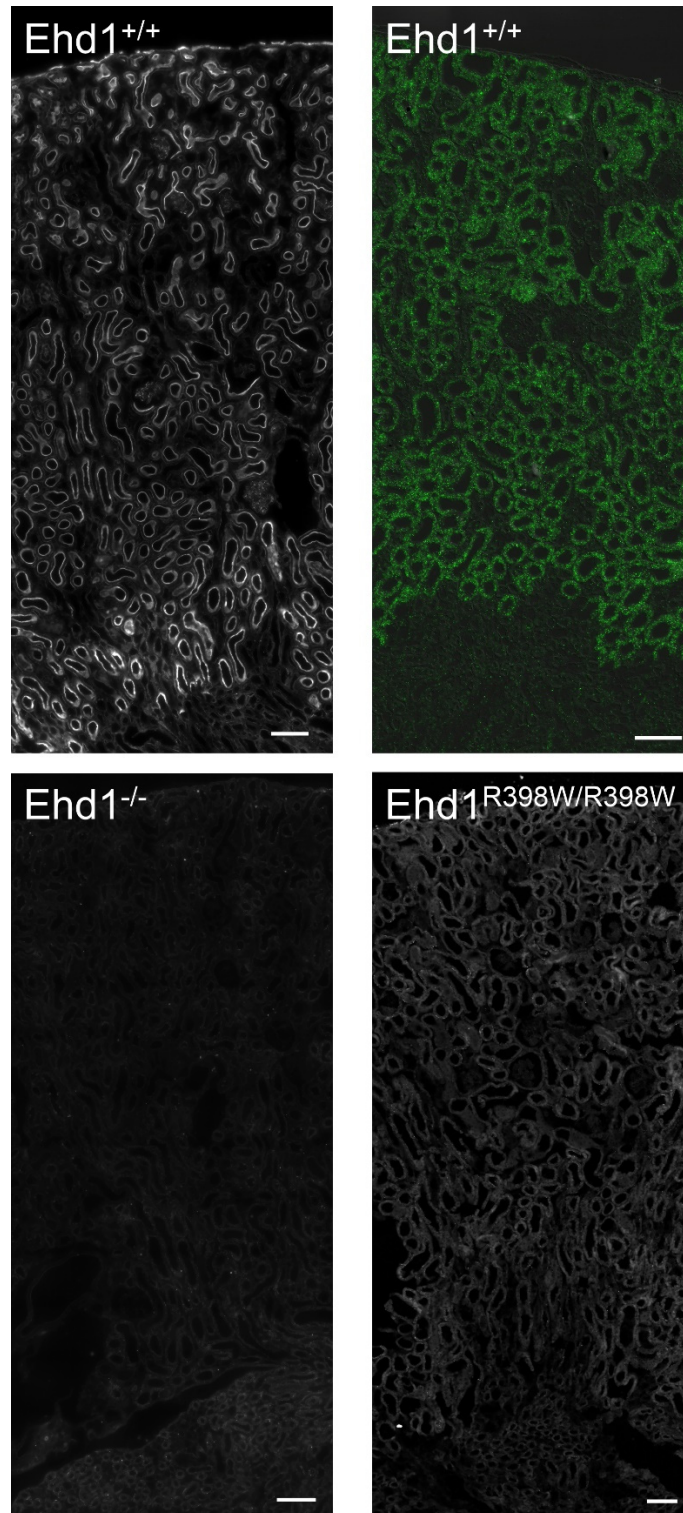
Supplemental Figures

Supplemental Figure 1: EHD1 in human kidney

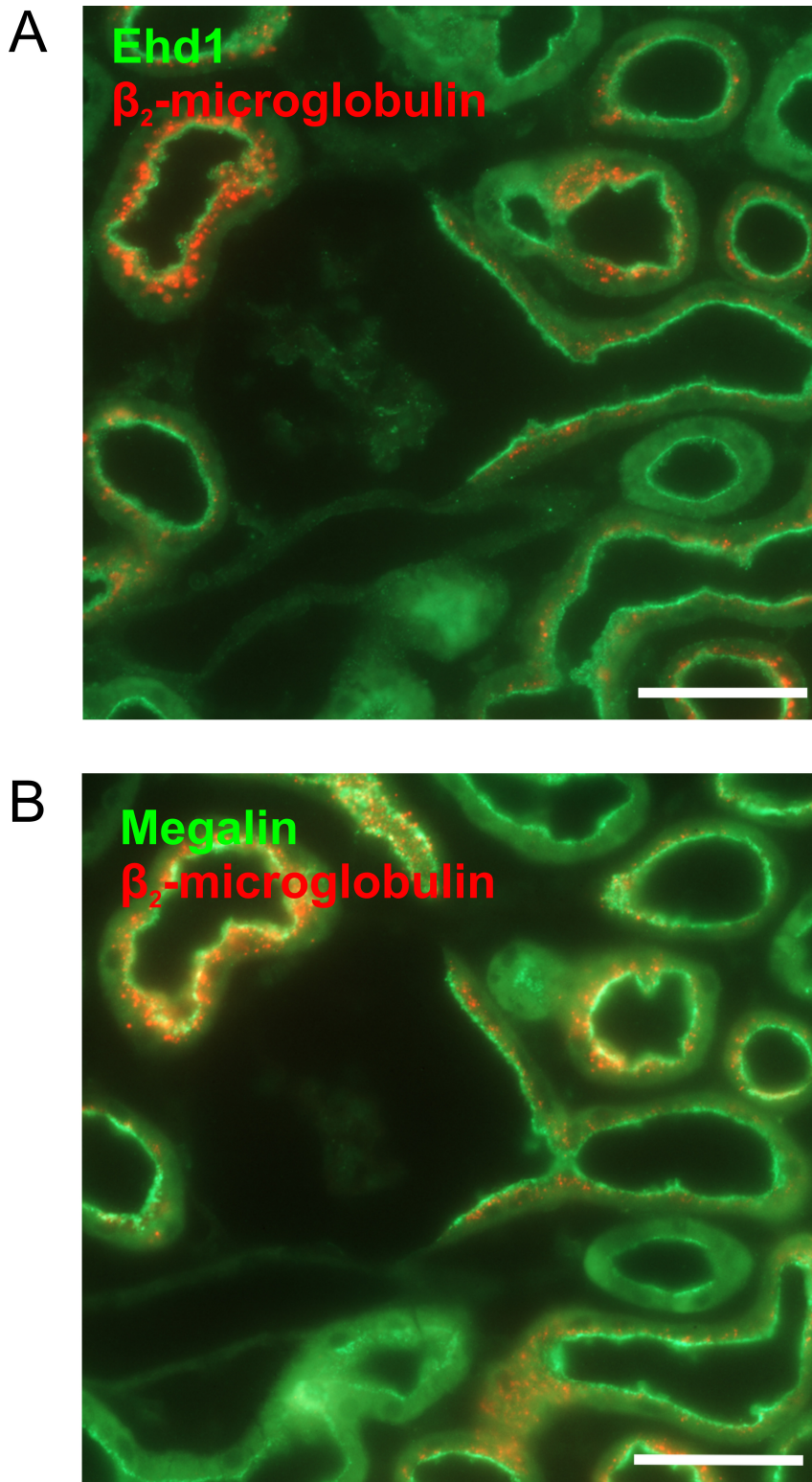


Localization of EHD1 (green) in normal human kidney. Aquaporin-2 is labeled in red. The middle panel and lower panel are magnifications of the areas marked in the upper panel. Strong EHD1-positive labeling was present in proximal tubules. Scale bar 500 μ m.

Supplemental Figure 2: Ehd1 in mouse kidney

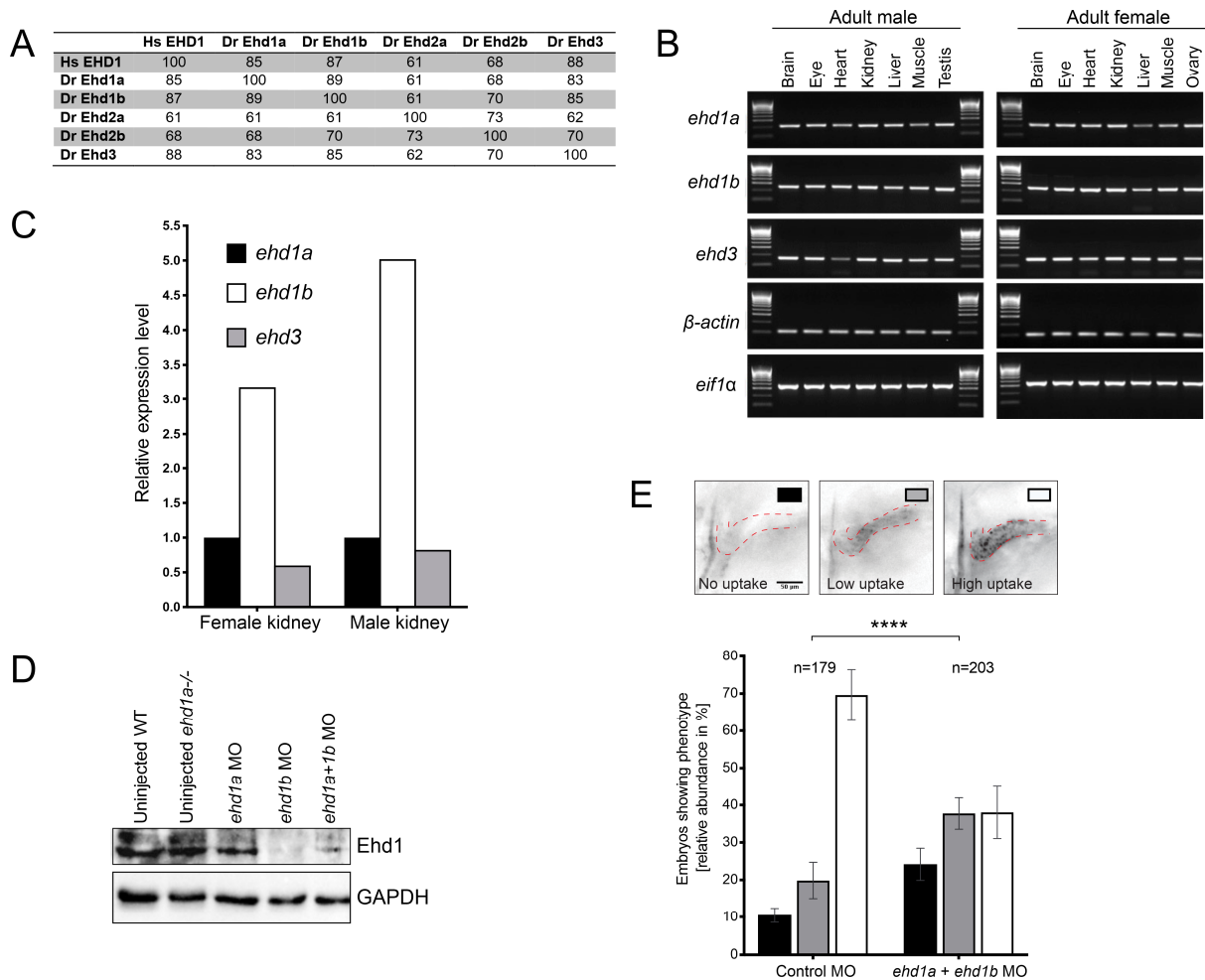


Similar to the localization in human kidney, Ehd1 was found in the apical/subapical compartment of proximal tubules using antibody staining (upper left panel) or RNAScope (upper right panel). In kidney cortex of a knockout mouse (lower left panel) no Ehd1-specific antibody staining was observed while knockin mouse showed limited granular staining (lower right panel). Scale bars 100 μ m.

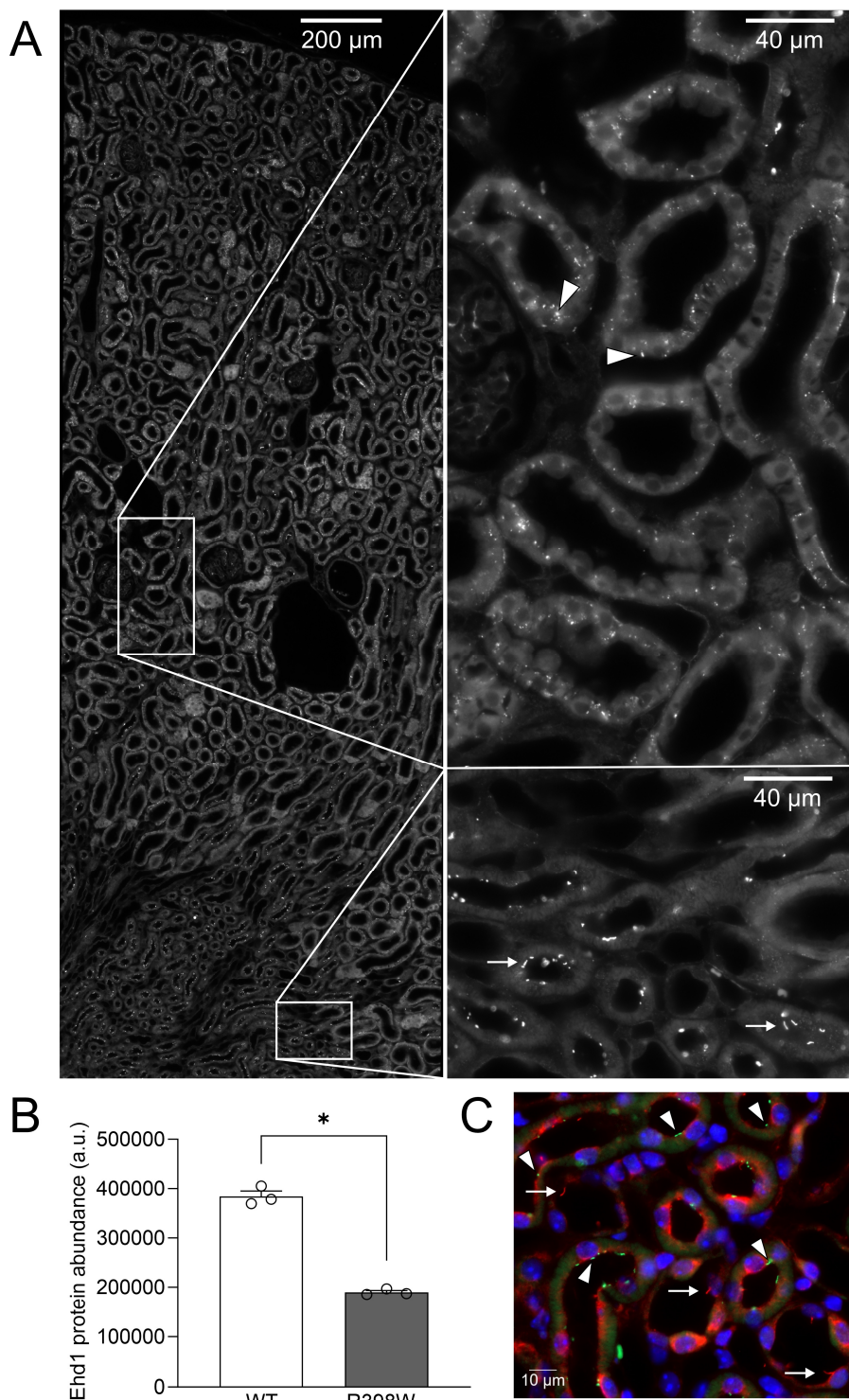
Supplemental Figure 3: Localization Ehd1, Megalin and reabsorbed β_2 -microglobulin

53 Ehd1 and Megalin show an overlapping subcellular localization. (A) Murine Ehd1 (green) was
54 immunostained in the kidney of a mouse that was injected with labeled β_2 -microglobulin (red) 30 min
55 prior to fixation. Please note localization of β_2 -microglobulin and Ehd1 in the apical/subapical
56 compartment. (B) In a consecutive section (lower panel), Megalin (green) is also localized in the
57 apical/subapical compartment. Scale bars: 50 μ m.
58
59
60

Supplemental Figure 4. Zebrafish

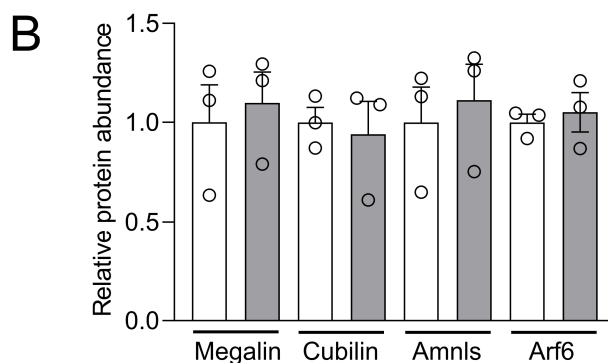
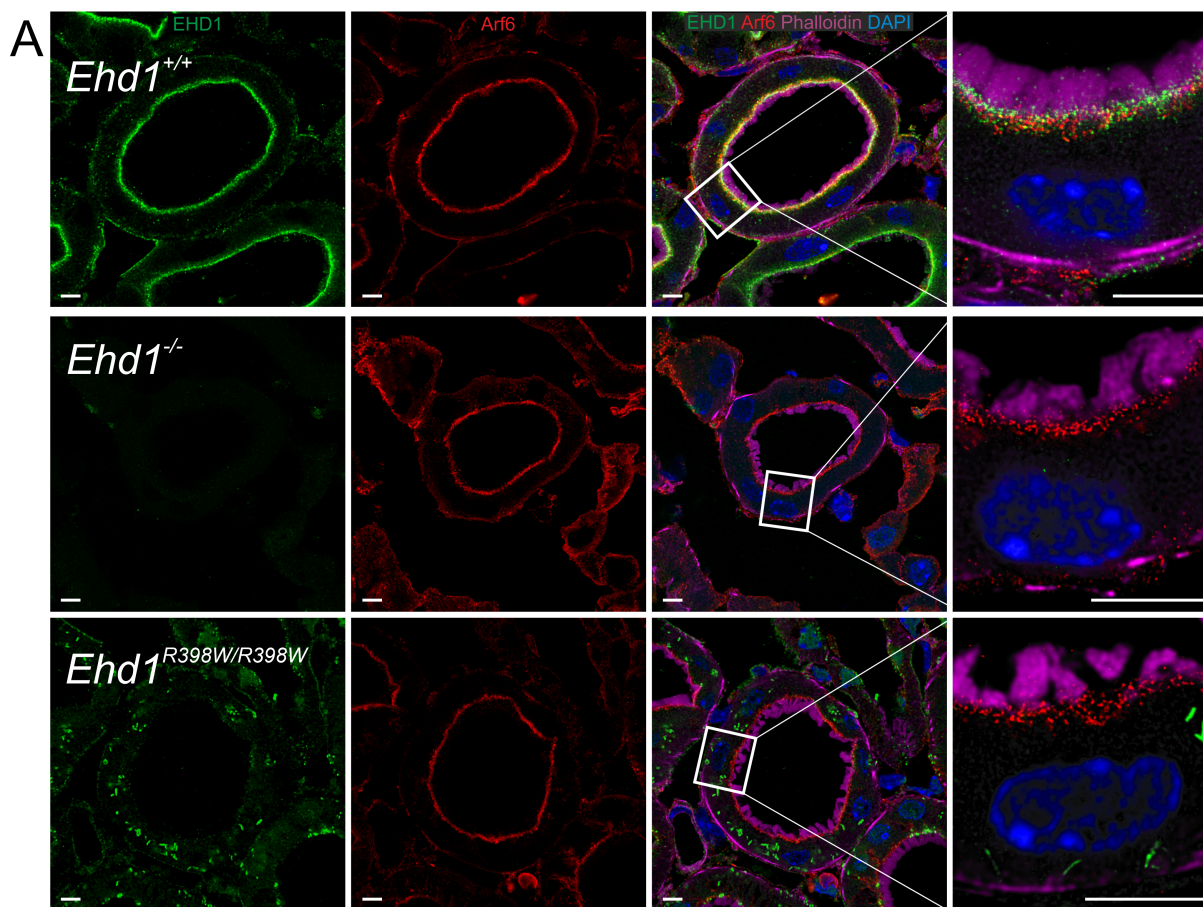


Expression analysis of zebrafish *ehd* orthologues and a role for Ehd1 in proximal tubular uptake. (A) Homology at the protein levels between human (Hs) EHD1 and the zebrafish (Dr) Ehd proteins. (B) RT-PCR analysis of tissue expression of zebrafish *ehd* transcripts. Shown is a representative PCR of tissue samples prepared from a total 18 animals, 3 biological replicates. (C) Q-PCR analysis of zebrafish *ehd1a*, *ehd1b* and *ehd3* expression in the adult zebrafish kidney. The Q-PCR was performed in duplicate, each time from samples prepared from 3 biological replicates. Values are normalized to the housekeeping gene *eif1a*. (D) Western blot of protein extracts from 3 dpf uninjected wildtype or *ehd1a*-null larvae or wildtype larvae injected with splice-blocking morpholinos to *ehd1a*, *ehd1b*, or both *ehd1a* and *ehd1b*. Ehd1a and b were detected with anti-EHD1 antibody. GAPDH is a loading control. Shown is a representative Western blot of samples prepared from approximately 100 larvae per condition. (E) Uptake of Alexa488-conjugated 10 kDa dextran into the pronephric tubules of 4 dpf zebrafish larvae treated with control morpholino (MO) or morpholinos targeting *ehd1a* and *ehd1b*. Uptake was assessed at 2.5 h post-injection by fluorescence stereomicroscopy and is scored as indicated. The bars correspond to the relative abundance of the different categorized phenotypes shown in the microscopy images (black, no uptake; grey, low uptake; white, high uptake). Data are presented as the mean \pm SEM. Statistical analysis was performed using the Pearson's chi-squared test. **** indicates $p \leq 0.0001$.

Supplemental Figure 5: Localization of Ehd1^{R398W} in mouse kidney

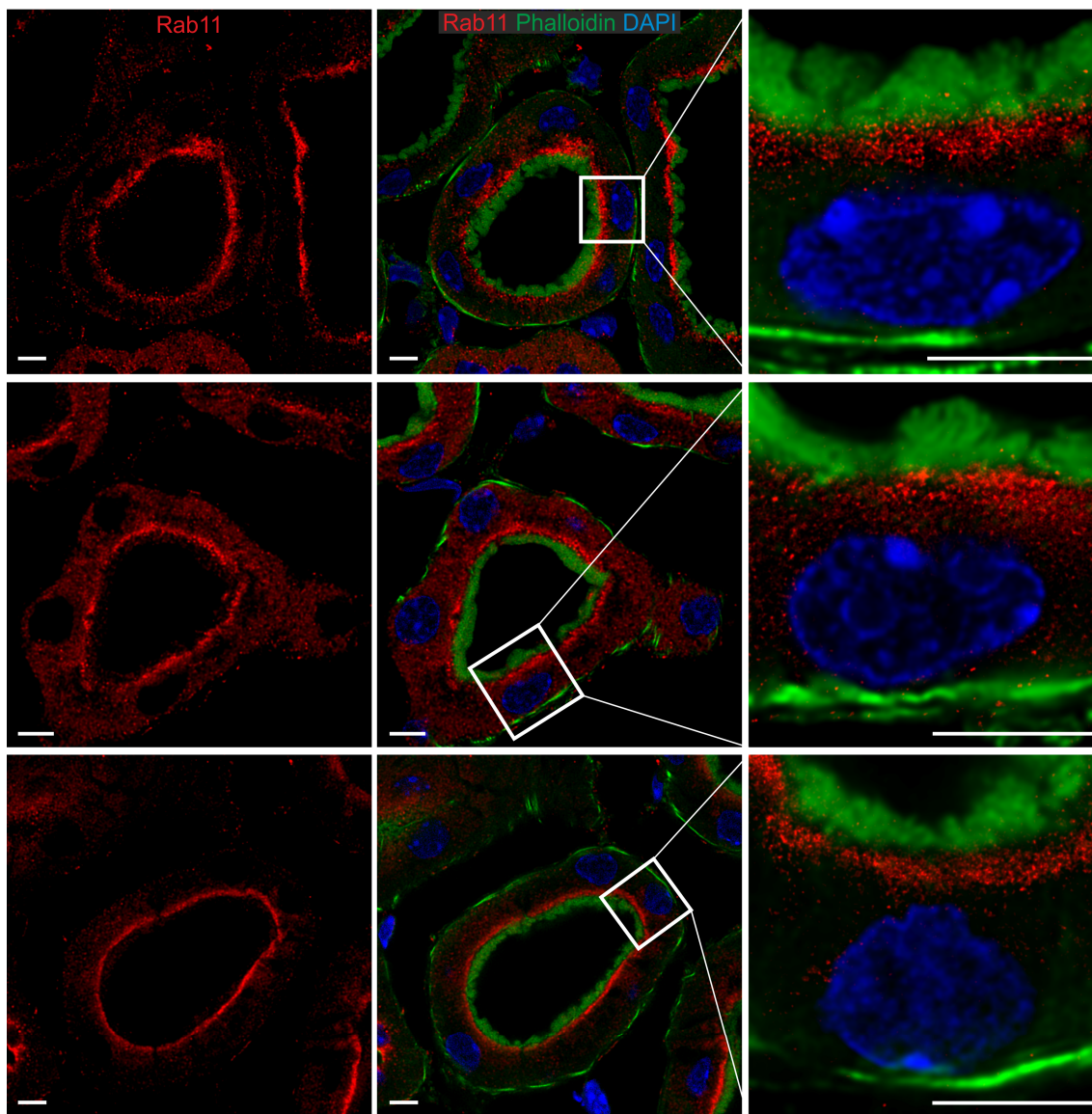
(A) In kidneys of homozygous *Ehd1*^{R398W/R398W} knockin mice, Ehd1-specific immunostaining was sparse and mainly localized in small aggregates within the proximal tubular cells (arrowheads). In distal segments such as thick ascending limbs, filament-like structures were found at the apical side (arrows). These Ehd1-positive apical structures were absent in wildtype mice and negative for acetylated tubulin. (B) Protein abundance determined by mass spectrometry of kidney lysates of wildtype and *Ehd1*^{R398W/R398W} mice revealed reduced Ehd1 protein abundance in knockin mice (n=3 each group). (C) No overlap between Ehd1-positive structures (green, arrowheads) and acetylated tubulin (red, arrows).

Supplemental Figure 6: Localization of Ehd1 and Arf6 in mouse kidneys



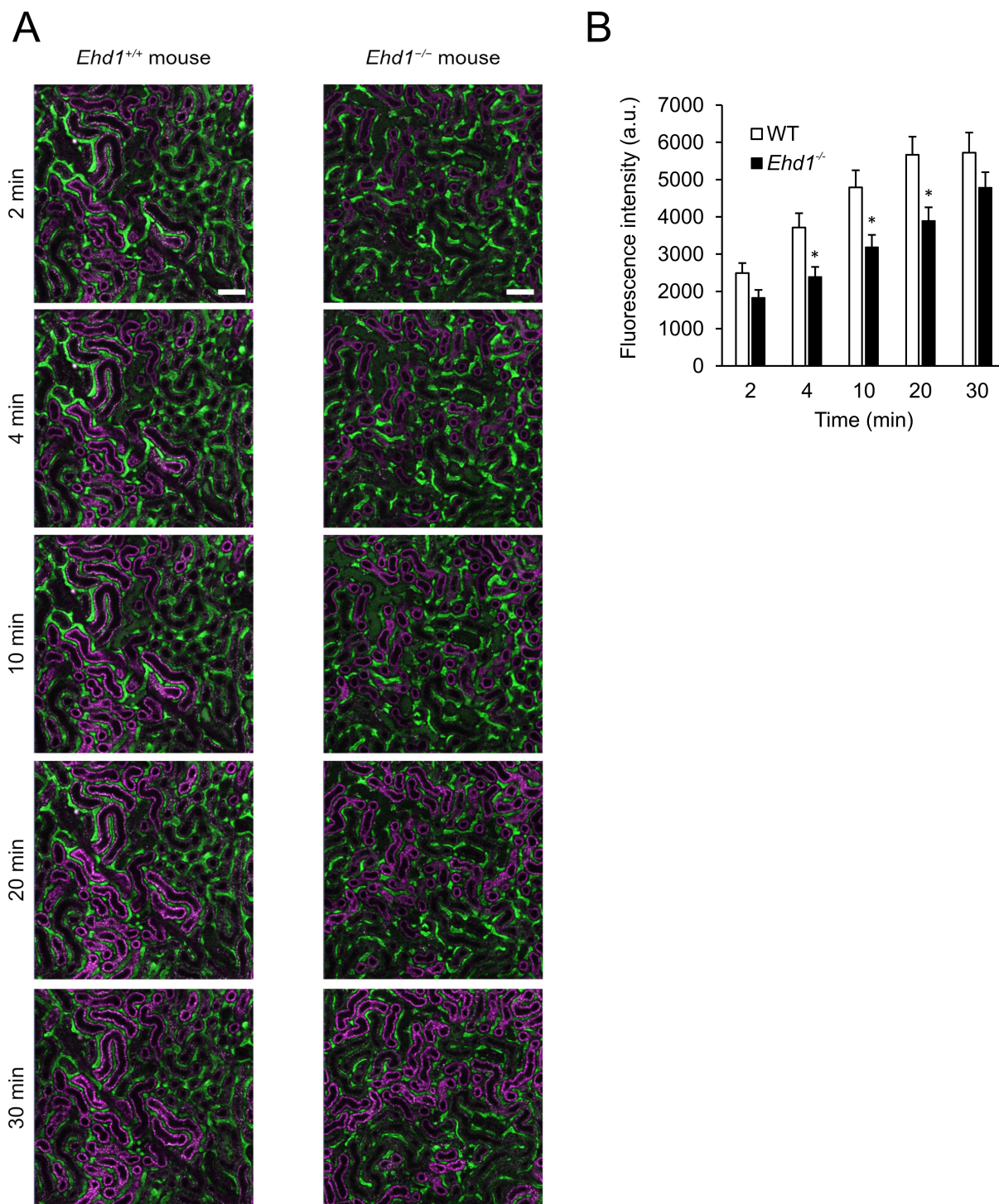
(A) Localization and abundance of Arf6 (red), a factor involved in trafficking of biological membranes and protein cargo, appeared to be similar in wildtype mouse kidney (upper panels), *Ehd1* knockout (middle panels) and *Ehd1*^{R398W/R398W} knockin mice (lower panel). *Ehd1* (green); Phalloidin (magenta) was used as a marker of the brushborder membrane; nuclei were stained with DAPI (blue). Left three panels: confocal images; right panel: STED image for *Ehd1* and Arf6. Deconvolution of all images using Huygens software. Scale bar: 5 μ m. (B) Relative protein abundance of Megalin, Cubilin, Amnionless (Amnls), and Arf6, determined by mass spectrometry of kidney lysates of wildtype (white bars) and *Ehd1*^{R398W/R398W} mice (gray bars). n=3 each group.

Supplemental Figure 7: Effect of *Ehd1* knockout and knockin on the localization of Rab11



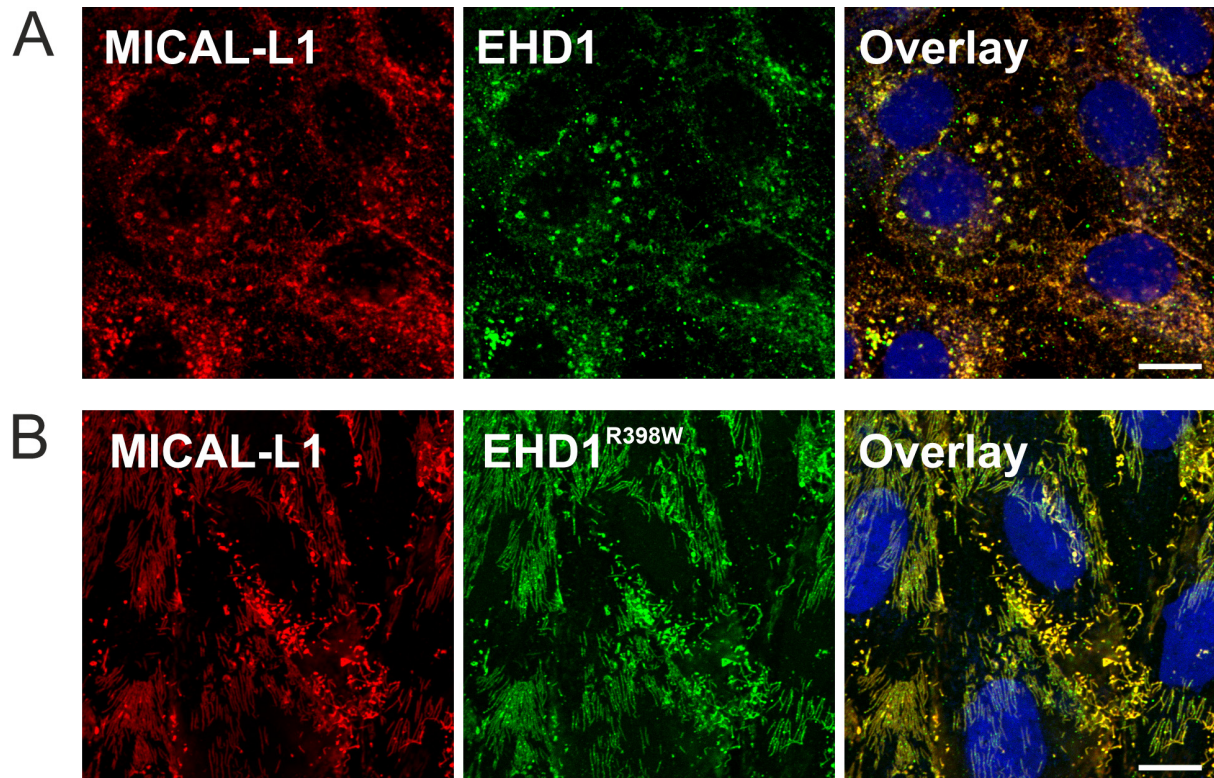
Localization and abundance of Rab11, a regulator of intracellular membrane trafficking routes, appeared to be similar in wildtype mouse kidney (upper panels), *Ehd1* knockout (middle panels) and *Ehd1^{R398W/R398W}* knockin mice (lower panel). Phalloidin (green) was used as a marker of the brushborder membrane; nuclei were stained with DAPI (blue). Left two panels: confocal images; right panel: STED image for Rab11. Deconvolution of all images using Huygens software. Scale bar: 5 μ m

Supplemental Figure 8: Intravital multiphoton microscopy

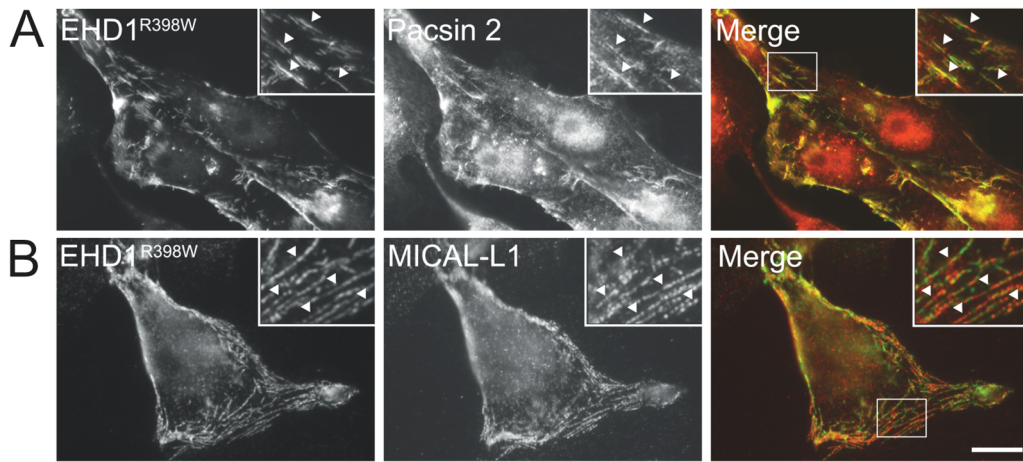


(A) Original intravital microscopy experiments illustrating the delayed reabsorption of labeled β_2 -microglobulin (magenta) in the kidney of an *Ehd1*^{-/-} mouse. Blood vessels are stained by FITC-coupled high molecular dextran (green). Scale bars 75 μ m. (B) Summary of experiments (6 animals each group, 31-36 tubules per group) as shown in (A) to illustrate the time course of the reduced rate of reabsorption. The data at 10 min are identical to the data shown in Figure 3G. Asterisks indicate $p \leq 0.05$.

Supplemental Figure 9: EHD1 and MICAL-L1 in EDH1-overexpressing LLC-PK1 cells

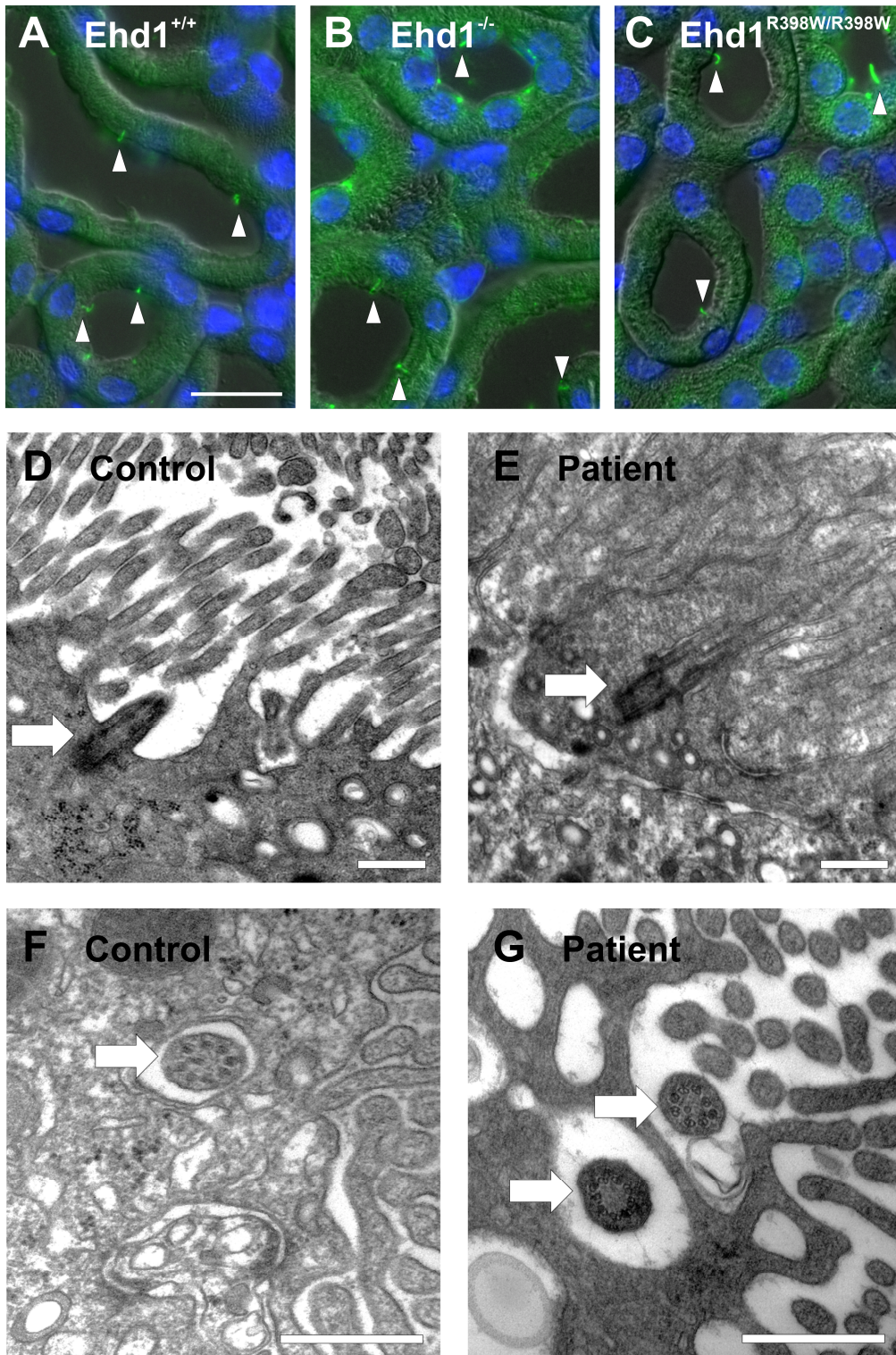


Immunofluorescence microscopy of LLC-PK1 cells expressing wildtype human EHD1 (A) or the EHD1^{R398W} mutant (B). MICAL-L1 (red) colocalized with EHD1 (green) in cells expressing wildtype and mutant EHD1. In the overlay images, cell nuclei were stained with DAPI (blue). Cells were induced for 48 h with doxycycline (1 mg/l). Scale bar: 10 μ m.

Supplemental Figure 10: MICAL-L1 and Pacsin 2 in cells overexpressing EDH1^{R398W}

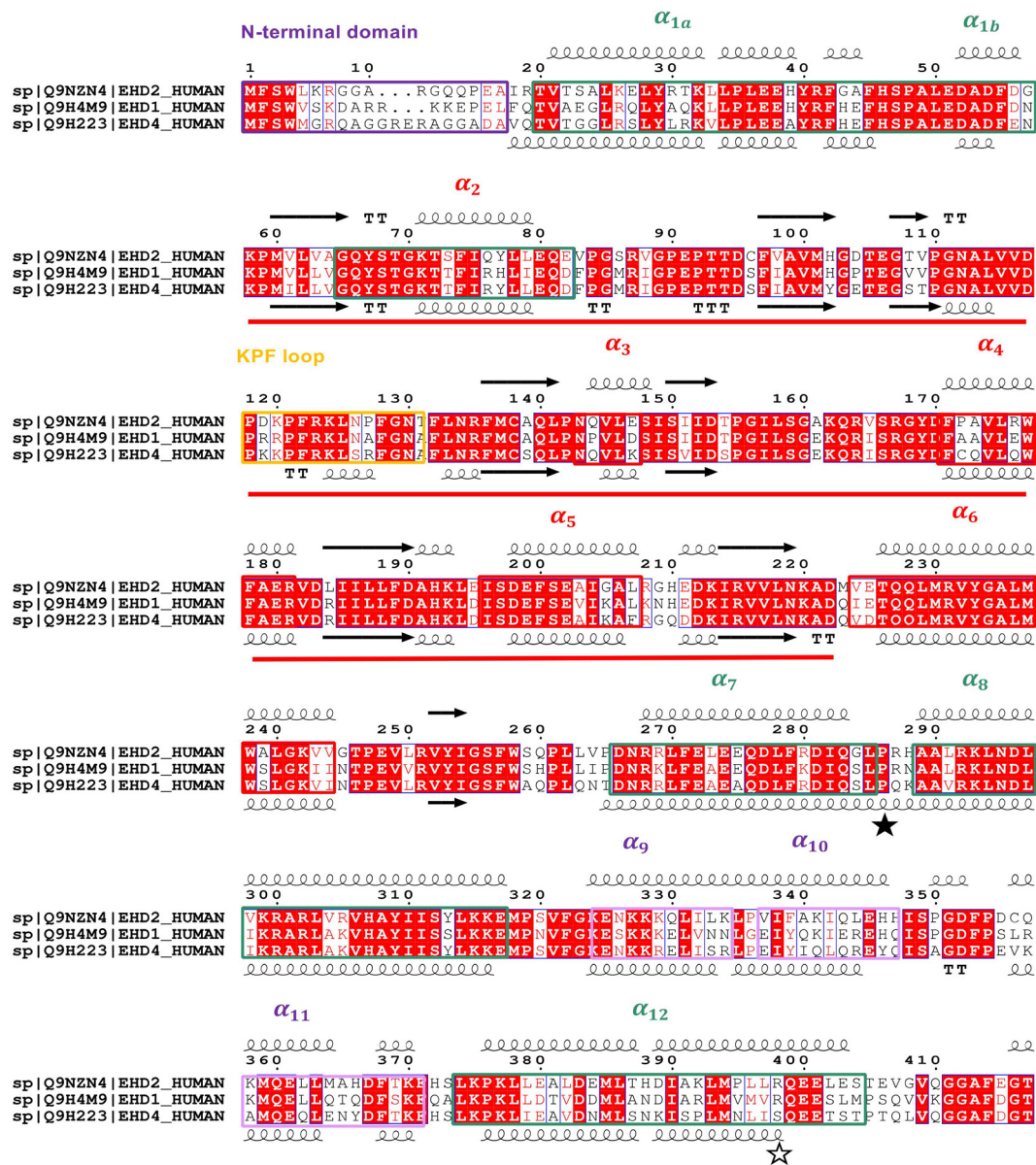
Immunofluorescence microscopy of LLC-PK1 cells expressing the EHDR398W mutant, labelled with antibodies to EHD1 and either Pacsin 2 (A) or MICAL-L1 (B) to label recycling endosomes. In the overlay images, EHD1 is shown in green, Pacsin 2 and MICAL-L1 in red. Arrowheads indicate colocalization within tubules. Cells were induced for 24 h with doxycycline. Scale bar: 20 μm .

Supplemental Figure 11: Primary cilia in murine and human kidneys



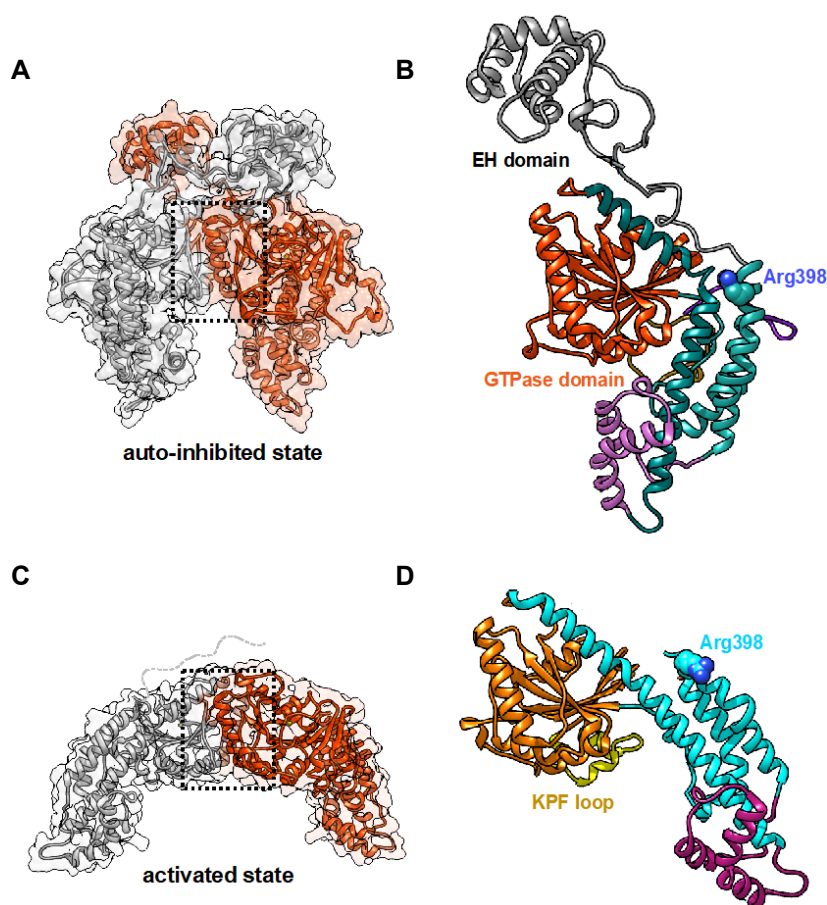
Proximal tubules of wildtype (A), homozygous *Ehd1* knockout (B), and R398W knockin mice (C) had similar numbers of Arl13b-positive primary cilia (arrow heads). Scale Bar 20 μ m. Electron microscopy (EM) of primary cilia (arrows) within human renal proximal tubules. EM normal kidney (D) / (F); EM affected individual (E) / (G). Please note, (D) and (E) show the base of cilia (longitudinal slice); (F) and (G) show a cross section of cilia. Scale Bars 500 nm.

Supplemental Figure 12: Alignment of EHD1, EHD2 and EHD4



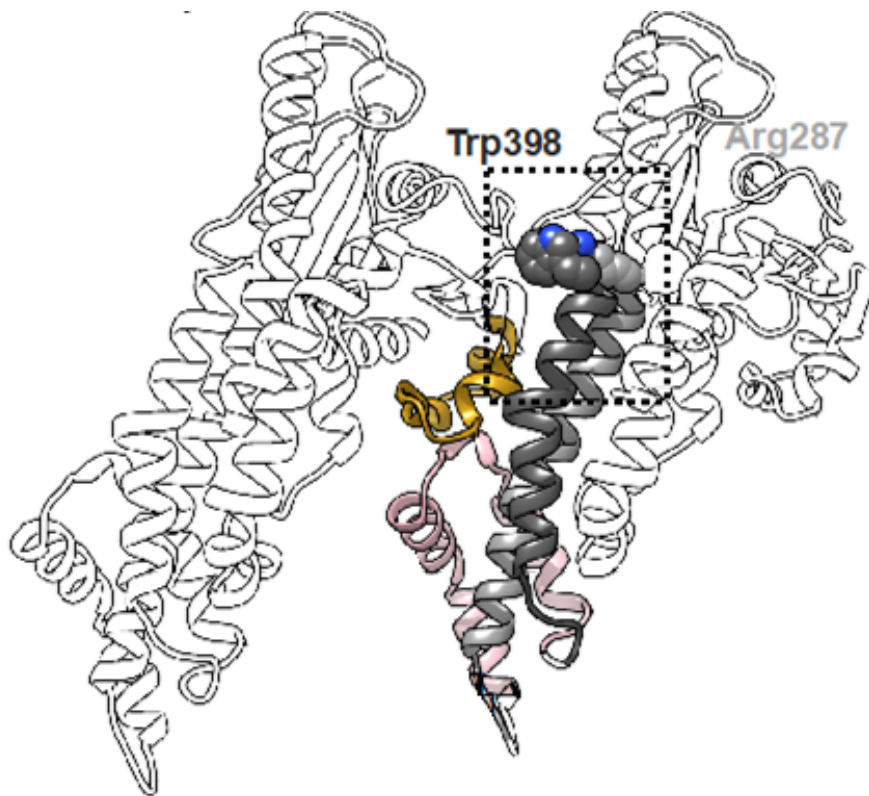
Multisequence alignment of human EHD1 (Q9H4M9), EHD2 (Q9NZN4) and EHD4 (Q9H223) by the program Clustal Omega reveals an overall identity between these isoforms of > 70%. The topology based on crystal structures of EHD2 (pdb entry code 4CDI) and EHD4 (pdb entry code 5MTV) is shown on top and bottom of the respective sequences. EHD proteins consist of an N-terminal unordered domain (purple), a small helical domain α_1 (dark cyan), the GTPase domain comprising α_2 - α_5 (red), several β -sheets (indicated as black arrows) and the dimerization interface helix α_6 . Adjacent to the GTPase domain is the helix pair α_7 - α_8 (dark cyan) separated by the hinge residue Pro286 (black star) and the membrane interacting helices α_9 - α_{11} (pink). Helix α_{12} connects to the EH-domain (not shown) via a long unordered linker loop. The mutation Arg398Trp in EHD1 is located at the very end of α_{12} (white star).

Supplemental Figure 13: Structural modeling: Putative structure of EHD1 dimers



Homology models of EHD1 determined by the program Modeller using the autoinhibited state of EHD2 (pdb entry code 4CDI) (A and B) and the activated state of EHD4 (pdb entry code 5MTV) (C and D) as a template, respectively. A and C: Similar to EHD2 and EHD4, EHD1 presumably forms stable dimers (monomers are colored in red and grey) with $\alpha 6$ serving as dimerization helix (box in dotted line). EH-domains are only resolved in the auto-inhibited state locking the ATPase domain of the neighboring monomer in the dimer. Although the EH-domain of EHD4 was present during crystallization it was not resolved suggesting that the blocking interaction was released during activation. Since EH domains were not resolved in the activated state, they are not shown in (C) and (D). The higher degree of flexibility is in agreement with the functional role of EH-domain as interaction partners for different proteins in the activated state. The domain structure in the EHD1 homology model is shown in the putative autoinhibited state (B) and the activated state (D). Arg398 is shown in sphere representation located at the end of $\alpha 12$. The KPF loop is only ordered in the activated state (colored in gold in (D)).

1
2
3 **Supplemental Figure 14: Structural modeling: Effects of the R398W mutation on EHD1**
4 **oligomerization**
5



35 Mutation of Arg398 against a bulky residue such as tryptophan probably disturbs the dimer-dimer
36 interaction between the KPF loop and the helical bundle and thereby prevents oligomerization. A
37 possible pathological interaction partner of Trp398 suggested from homology modelling would be
38 Arg287, which would strengthen the interactions between α_{12} and α_8 within one monomer.
39
40
41
42
43
44
45
46
47
48
49
50
51
52
53
54
55
56
57
58
59
60

Supplemental References

1. Cebrian-Serrano A, Zha S, Hanssen L, Biggs D, Preece C, Davies B: Maternal Supply of Cas9 to Zygotes Facilitates the Efficient Generation of Site-Specific Mutant Mouse Models. *PLoS One* 12: e0169887, 2017 doi: 10.1371/journal.pone.0169887
2. Theilig F, Kriz W, Jerichow T, Schrade P, Hahnel B, Willnow T, et al.: Abrogation of protein uptake through megalin-deficient proximal tubules does not safeguard against tubulointerstitial injury. *J Am Soc Nephrol* 18: 1824-1834, 2007
3. Marshansky V, Bourgoin S, Londono I, Bendayan M, Vinay P: Identification of ADP-ribosylation factor-6 in brush-border membrane and early endosomes of human kidney proximal tubules. *Electrophoresis* 18: 538-547, 1997
4. Schilling A, Gerum R, Krauss P, Metzner C, Tziridis K, Schulze H: Objective Estimation of Sensory Thresholds Based on Neurophysiological Parameters. *Front Neurosci* 13: 481, 2019 doi: 10.3389/fnins.2019.00481
5. Lu Q, Insinna C, Ott C, Stauffer J, Pintado PA, Rahajeng J, et al.: Early steps in primary cilium assembly require EHD1/EHD3-dependent ciliary vesicle formation. *Nat Cell Biol* 17: 228-240, 2015 doi: 10.1038/ncb3109
6. Oltrabella F, Pietka G, Ramirez IB, Mironov A, Starborg T, Drummond IA, et al.: The Lowe syndrome protein OCRL1 is required for endocytosis in the zebrafish pronephric tubule. *PLoS Genet* 11: e1005058, 2015 doi: 10.1371/journal.pgen.1005058
7. Fischer R, Kessler BM: Gel-aided sample preparation (GASP)--a simplified method for gel-assisted proteomic sample generation from protein extracts and intact cells. *Proteomics* 15: 1224-1229, 2015 doi: 10.1002/pmic.201400436
8. Reinders J, Altenbuchinger M, Limm K, Schwarzfischer P, Scheidt T, Strasser L, et al.: Platform independent protein-based cell-of-origin subtyping of diffuse large B-cell lymphoma in formalin-fixed paraffin-embedded tissue. *Sci Rep* 10: 7876, 2020 doi: 10.1038/s41598-020-64212-z
9. Gillet LC, Navarro P, Tate S, Rost H, Selevsek N, Reiter L, et al.: Targeted data extraction of the MS/MS spectra generated by data-independent acquisition: a new concept for consistent and accurate proteome analysis. *Mol Cell Proteomics* 11: O111 016717, 2012 doi: 10.1074/mcp.O111.016717
10. Simburger JMB, Dettmer K, Oefner PJ, Reinders J: Optimizing the SWATH-MS-workflow for label-free proteomics. *J Proteomics* 145: 137-140, 2016 doi: 10.1016/j.jprot.2016.04.021
11. Daumke O, Lundmark R, Vallis Y, Martens S, Butler PJ, McMahon HT: Architectural and mechanistic insights into an EHD ATPase involved in membrane remodelling. *Nature* 449: 923-927, 2007 doi: 10.1038/nature06173
12. Melo AA, Hegde BG, Shah C, Larsson E, Isas JM, Kunz S, et al.: Structural insights into the activation mechanism of dynamin-like EHD ATPases. *Proc Natl Acad Sci U S A* 114: 5629-5634, 2017 doi: 10.1073/pnas.1614075114

1
2
3
4
5
6
7
8
9
10
11
12
13
14
15
16
17
18
19
20
21
22
23
24
25
26
27
28
29
30
31
32
33
34
35
36
37
38
39
40
41

A Founder Mutation in EHD1 Presents with Tubular Proteinuria and Deafness

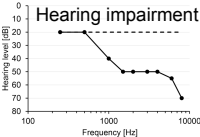
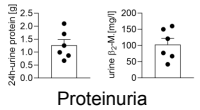
METHODS

Homozygous R398W mutation of the membrane-shaping protein EHD1 in six patients with tubular proteinuria and deafness.

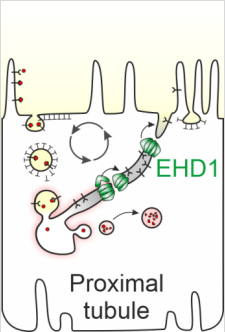
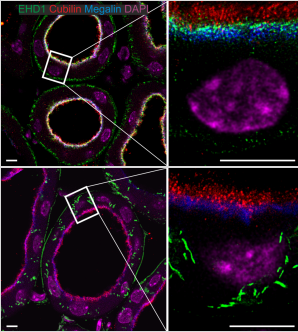
Disease mechanisms were analyzed using genetics, cell biology, structural biology, zebrafish and mouse models.

Conclusion

Based on six patients with proteinuria and hearing deficit, EHD1 was identified as a critical component of the renal protein reabsorption machinery and inner ear function.



OUTCOME



doi: 10.1681/ASN.2021101312